

1 Plateaus and jumps in the atmospheric radiocarbon record – Potential origin and value
2 as global age markers for glacial-to-deglacial paleoceanography, a synthesis

3
4
5 Michael Sarnthein¹⁾, Kevin Küssner²⁾, Pieter M. Grootes³⁾, Blanca Ausin⁴⁾⁸⁾, Timothy
6 Eglinton⁸⁾, Juan Muglia⁵⁾, Raimund Muscheler⁶⁾, Gordon Scholout⁷⁾

7
8
9 1) Institute of Geosciences, University of Kiel, Olshausenstr. 40, 24098 Kiel, Germany,
10 michael.sarnthein@ifg.uni-kiel.de (*corresponding author*)

11 2) Alfred-Wegener-Institut Helmholtz-Zentrum für Polar- und Meeresforschung,
12 Department for Marine Geology, 27570 Bremerhaven, Germany, kevin.kuessner@awi.de

13 3) Institute of Ecosystem Research, University of Kiel, Olshausenstr. 40, 24098 Kiel,
14 Germany, pgrootes@ecology.uni-kiel.de

15 4) Geology Department, University of Salamanca, Plaza de los Caldos, 37008
16 Salamanca, Spain, <ausin@usal.es>

17 5) Centro para el Estudio de los Sistemas Marinos, CONICET, 2915 Boulevard Brown,
18 U9120ACD, Puerto Madryn, Argentina, jmuglia@cenpat-conicet.gob.ar

19 6) Quaternary Sciences, Department of Geology Lund University, Sölvegatan 12, 22362
20 Lund, Sweden, raimund.muscheler@geol.lu.se

21 7) Climate Dynamics and Landscape Evolution, GFZ German Centre for Geosciences,
22 Telegrafenberg, 14473 Potsdam, Germany, ScholoutG@gmail.com

23 8) Geological Institute, ETH Zürich, Sonneggstr. 5, 8092 Zuerich, Switzerland,

24
25
26 [final version submitted to CLIMATE OF THE PAST \(2020-11-12\)](#)

27
28

29 ABSTRACT

30 Changes in the geometry of ocean Meridional Overturning Circulation (MOC) are crucial in
31 controlling past changes of climate and the carbon inventory of the atmosphere. However, the
32 accurate timing and global correlation of short-term glacial-to-deglacial changes of MOC in
33 different ocean basins still present a major challenge. The fine structure of jumps and plateaus
34 in atmospheric and planktic radiocarbon (^{14}C) concentration reflects changes in atmospheric ^{14}C
35 production, ocean-atmosphere ^{14}C exchange, and ocean mixing. Plateau boundaries in the
36 atmospheric ^{14}C record of Lake Suigetsu, now tied to Hulu U/Th model-ages instead of optical
37 varve counts, provide a stratigraphic 'rung ladder' of up to 30 age tie points 29 to 10 cal. ka for
38 accurate dating of planktic oceanic ^{14}C records. The age differences between contemporary
39 planktic and atmospheric ^{14}C plateaus record the global distribution of ^{14}C reservoir ages for
40 surface waters of the Last Glacial Maximum (LGM) / deglacial Heinrich Stadial 1 (HS-1), as
41 documented in 19/20 planktic ^{14}C records. Elevated and variable reservoir ages mark both
42 upwelling regions and high-latitude sites covered by sea ice and/or meltwater. ^{14}C ventilation
43 ages of LGM deep waters reveal opposed geometries of Atlantic and Pacific MOC. Like today,
44 Atlantic deep-water formation went along with an estuarine inflow of old abyssal waters from the
45 Southern Ocean up to the northern North Pacific and an outflow of upper deep waters. During
46 early HS-1, ^{14}C ventilation ages suggest a reversed MOC and ~1500 year-long flushing of the
47 deep North Pacific up to the South China Sea, when estuarine circulation geometry marked the
48 North Atlantic, gradually starting near 19 ka. High ^{14}C ventilation ages of LGM deep waters
49 reflect a major drawdown of carbon from the atmosphere. The subsequent major deglacial age
50 drop reflects changes in MOC accompanied by massive carbon releases to the atmosphere as
51 recorded in Antarctic ice cores. These new features of MOC and the carbon cycle provide
52 detailed evidence in space and time to test and refine ocean models that, in part because of
53 insufficient spatial model resolution and reference data, still poorly reproduce our data sets.

54

55

56 1. INTRODUCTION

57 1.1 A variety of terms linked to the notion '¹⁴C age'

58 The ¹⁴C concentration in the troposphere is mainly determined by ¹⁴C production,
59 atmospheric mixing, moreover, air-sea gas exchange and ocean circulation that vary
60 over time (e.g., Alves et al., 2018; Alveson et al., 2018). The ¹⁴C content of living
61 terrestrial plants is in equilibrium with the atmosphere via processes of photosynthesis
62 and respiration. Accordingly, the ¹⁴C of terrestrial plant remains in a sediment section
63 directly reflects the amount of radioactive decay, thus the time passed since the plant's
64 death, and the ¹⁴C composition of the atmosphere during the time of plant growth.

65

66 Contrariwise, ¹⁴C values of marine and inland waters are cut off from cosmogenic ¹⁴C
67 production in the atmosphere, hence depend on the carbon transfer at the air-water
68 interface and the result of local transport and mixing of carbon in the water. For surface
69 waters, the air-sea transfer involves a time span of ten years and less (e.g., Nydal et al.,
70 1998). Yet, vertical and horizontal water mixing results in surface ocean ¹⁴C
71 concentrations on average 5 % lower than those in the contemporaneous atmosphere,
72 a difference expressed as 'Marine Reservoir Age' (or 'reservoir effect' *sensu* Alves et
73 al., 2018). These 'ages' reflect the local oceanography and are highly variable through
74 time (~200–2500 yr; e.g., Stuiver and Braziunas, 1993; Grootes and Sarnthein, 2006;
75 Sarnthein et al., 2015). Apart from U/Th dated corals (many papers on their reservoir
76 age since Adkins and Boyle, 1997), the ¹⁴C age of planktic foraminifers is the most
77 common tracer in marine sediments providing a rough estimate of the time passed
78 since sediment deposition. Soon, however, marine geologists were confronted with age
79 inconsistencies that implied a series of unknowns, in particular the surface ocean ¹⁴C
80 'reservoir age' that finally became a most valuable tracer for oceanography.

81

82 The ^{14}C records of benthic foraminifers in deep-sea sediments reflect the time of
83 radioactive decay since their deposition with the apparent 'ventilation age' of the deep
84 waters in which they lived. Ventilation age is primarily the time span from the moment
85 when carbon dissolved in the local surface waters with somewhat reduced ^{14}C level lost
86 contact with the atmosphere until the precipitation of benthic carbonate from the down-
87 welled deep waters. Details on the derivation of ventilation ages are provided in Cook
88 and Keigwin (2015) and Balmer and Sarnthein (2018). In addition, however, ventilation
89 ages include hardly quantifiable lateral admixtures of older and/or younger water
90 masses, moreover, ^{14}C -enriched organic carbon supplied by the biological pump, thus
91 are called 'apparent'. Today, the apparent transit times of carbon dissolved in the deep
92 ocean range from a few hundred up to ~ 1800 ^{14}C yr found in upper deep waters of the
93 northeastern North Pacific (Matsumoto, 2007).

94

95 The reservoir ages of surface waters and the ventilation ages of deep waters present
96 robust and high-resolution tracers essential for drawing quantitative conclusions on past
97 ocean circulation geometries, marine climate change, and the processes that drive both
98 past ocean dynamics and carbon budgets, given the ages rely on a number of robust
99 age tie points. Obtaining such tie points presents a problem, since any attempt to date a
100 deep-sea sediment record by means of ^{14}C encounters a number of intricacies of how to
101 disentangle the effects of global atmospheric ^{14}C variations due to past changes in
102 cosmogenic ^{14}C production and carbon cycle from (i) local depositional effects such as
103 sediment hiatuses and winnowing, differential bioturbational mixing depth, and sediment
104 transport by deep burrows, (ii) the effects of local atmosphere-ocean exchange and
105 ocean mixing resulting in reservoir and ventilation ages that change through time and

106 space (e.g., Alves et al. 2018; Grootes and Sarnthein, 2006), and (iii) from the final
107 target, quantitatively 'pure' ^{14}C ages due to radioactive decay. These problems are
108 exacerbated by the need for a generally accepted high-precision atmospheric reference
109 record for the period 14–50 cal. ka, beyond tree ring calibration,
110
111 Current ^{14}C -based chronologies of deep-sea sediment records, used to constrain and
112 correlate the age of glacial-to-deglacial changes in ocean dynamics and climate on a
113 global scale, are often of insufficient quality when they are based on (i) age tie points
114 spaced far too wide (e.g., using DO-events 1, 2, and 3 only and/or sporadic tephra
115 layers for the time span 30–14 cal ka), (ii) disregarding atmospheric ^{14}C plateaus, (iii)
116 the risky assumption of \pm constant planktic ^{14}C reservoir ages and other speculative
117 stratigraphic correlations/compilations, and (iv) ignoring small-scale major differences in
118 low-latitude reservoir age. Likewise, clear conclusions are precluded by an uncertainty
119 range of 3–4 kyr sometimes accepted for tie points during the glacial-to-deglacial period
120 (Stern and Lisiecki, 2013; Lisiecki and Stern, 2016), where significant global climate
121 oscillations occurred on decadal-to-centennial time scales as widely shown on the basis
122 of speleothem and ice core-based records (Steffensen et al., 2008; Svensson et al.,
123 2008; Wang et al., 2001). Thus marine paleoclimate and paleoceanographic studies
124 today focus on the continuing quest for a high-resolution and global, hence necessarily
125 atmospheric ^{14}C reference record.

126

127 *1.2 Review of tie points used to fix calibrated and reservoir ages in marine ^{14}C records*

128 The tree ring-based calibration of ^{14}C ages provides a master record of decadal
129 changes in atmospheric ^{14}C concentrations back to ~14 cal. ka (Reimer et al., 2013 and
130 2020) with floating sections beyond (from ~12.5–14.5 cal. ka, around 29–31.5 and 43

131 cal. ka; Turney et al., 2010, 2017, Reimer et al., 2020). The evolution of Holocene and
132 late deglacial ^{14}C ages with time is not linear but reveals variations with numerous
133 distinct jumps (= rapid change) and (short) plateau-shaped (slow or no change or even
134 inversion) structures indicative of fluctuations in atmospheric ^{14}C concentration. Prior to
135 8500 cal. yr BP, various plateaus extend over 400–600 cal. yr and beyond (Fig. 2).
136 Given the quality of the tree ring calibration data, these fluctuations can be considered
137 real, suitable for global correlation (Sarnthein et al., 2007, 2015; Umling and Thunnell,
138 2017; Sarnthein and Werner, 2018). Air-sea gas exchange transfers the atmospheric
139 ^{14}C fluctuations into the surface ocean where they can provide high-resolution tie points
140 to calibrate the marine ^{14}C record and marine reservoir ages back to ~14 ka (via " ^{14}C
141 wiggle matching"). In the near future, however, it is unlikely that a continuous tree ring-
142 based record will become available to trace such atmospheric ^{14}C variations further
143 back, over the period 14–29 cal. ka crucial for the understanding of last-glacial-to-
144 interglacial changes in climate. Hence various other, carbonate-based ^{14}C archives
145 have been employed for this period to reconstruct past changes in atmospheric ^{14}C
146 concentration/age and tie them to an 'absolute' or 'calibrated' (e.g., incremental and/or
147 based on speleothem carbonate) age scale.

148

149 Suites of ^{14}C ages of paired marine and terrestrial plant-borne samples, e.g. paired
150 planktic foraminifers and wood chunks, provide most effective but rarely realizable
151 absolute-age markers and reservoir ages of local ocean surface waters (Zhao and
152 Keigwin, 2018; Rafter et al., 2018; Schroeder et al., 2016; Broecker et al., 2004).
153 Likewise successful appears the alignment of ^{14}C -dated variations in downcore sea-
154 surface temperatures (SST) with changes in hydroclimate as recorded in age-calibrated
155 sedimentary leaf-wax hydrogen isotope (δD) records from ancient lakes (Muschitiello et

156 al., 2019), assumed to be coeval. Further tie points are derived from volcanic ash layers
157 (Waelbroeck et al., 2001; Siani et al., 2013; Davies et al., 2014; Sikes and Guilderson,
158 2016), paired U/Th- and ^{14}C -based coral ages (Adkins and Boyle, 1997; Robinson et al.,
159 2005; Burke and Robinson, 2012; Chen et al., 2015), and the (fairly fragmentary)
160 alignment of major tipping points in ^{14}C dated records of marine SST and planktic $\delta^{18}\text{O}$
161 to the incremental age scale of climate events dated in polar ice core records
162 (Waelbroeck et al., 2011). Such well-defined tie points, however, are wide-spaced in
163 peak glacial-to-early deglacial ice core records, too wide for properly resolving a clear
164 picture of the spatiotemporal pattern of marine paleoclimate events. Finally, various
165 data compilations tentatively rely on the use of multiple age correlations amongst
166 likewise poorly dated marine sediment records, an effort necessarily problematic.
167 Skinner et al. (2019) recently combined new and existing reservoir age estimates from
168 North Atlantic and Southern Ocean to show coherent but distinct regional reservoir age
169 trends in subpolar ocean regions, trends that indeed envelop the range of actual major
170 small-scale and short-term oscillations in reservoir age revealed by our technique of ^{14}C
171 plateau tuning for the subpolar South Pacific (Küssner et al., under review).

172

173 Lacking robust age tie points several authors resort to ^{14}C reservoir age simulations for
174 various sea regions by ocean General Circulation Models (GCM) (e.g. Butzin et al.,
175 2017; Muglia et al., 2018) to quantify the potential difference between marine and
176 atmospheric ^{14}C dates for glacial-to-interglacial times. In view of the complexity of ocean
177 MOC and the global carbon cycle it is not surprising that the results of a comparison of
178 a selection of robust empiric vs. simulated ^{14}C reservoir ages are not that encouraging
179 yet (as discussed further below).

180

181 Beyond accepting a generally close link between ^{14}C concentrations in the troposphere
182 and in the surface ocean, the fine structure of planktic ^{14}C records with centennial-scale-
183 resolution can provide a far superior (though costly) link of the marine sediment records
184 to the reference suite of narrow-standing jumps and boundaries of the plateaus robustly
185 identified in the atmospheric ^{14}C record of Lake Suigetsu, the only long, continuous
186 record based on terrestrial plant remains (Bronk Ramsey et al., 2012, 2019). Beyond
187 the reach of the tree ring-based age scale ~ 14 cal. ka, the absolute age of the Suigetsu
188 atmospheric ^{14}C structures can be either calibrated by incremental (microscopy- or
189 XRF-based) varve counts (Scholaut et al., 2018; Marshall et al., 2012) or by a series of
190 paired U/Th- and ^{14}C -based model ages correlated from the Hulu Cave speleothem
191 record (Bronk Ramsey, 2012 and 2019; Southon et al., 2012; Cheng et al., 2018). The
192 difference in absolute age between these calibrations (Fig. 3) is of little importance for
193 the tuning of planktic to corresponding atmospheric ^{14}C plateaus and the derivation of
194 planktic reservoir ages that present the highly variable offset of the ^{14}C age of a planktic
195 plateau from that of the correlated atmospheric plateau. The offset is deduced by
196 subtracting the average ^{14}C age of an atmospheric ^{14}C plateau from that of the
197 correlated planktic ^{14}C plateau, independent of any absolute age value assigned.

198

199 The uncertainty of the Suigetsu atmospheric ^{14}C record is significantly larger than that
200 of the tree ring-based calibration record because of lower ^{14}C concentrations, limited
201 sampling density, and uncertainties in the independent age determination. Thus the ^{14}C
202 fluctuations could be real or represent mere statistical scatter (null hypothesis) in which
203 case the record of atmospheric ^{14}C ages against time would show a simple continuous
204 rise resulting from radioactive decay and the advance of time, such as suggested by a

205 fairly straight progression of the highly resolved deglacial Hulu Cave ^{14}C record plotted
206 vs. U/Th ages (Southon et al., 2012; Cheng et al., 2018).

207

208 The unequivocal fluctuations in the tree ring-based master record of atmospheric ^{14}C
209 concentration (Fig. 2; Reimer et al., 2013, 2020) are on the order of 2–3 % over the last
210 10 kyr (Stuiver and Braziunas, 1993) and even larger back to ~14 ka. Under glacial and
211 deglacial low- CO_2 conditions beyond 14 ka, when climate and ocean dynamics were
212 less constant than during the Holocene, real atmospheric ^{14}C fluctuations were, most
213 likely, even stronger and ^{14}C plateaus and jumps accordingly larger. Plateau-jump
214 structures are also becoming increasingly evident in the evolving atmospheric
215 calibration record (Reimer et al., 2020). The age-defined plateaus and jumps in the
216 Suigetsu atmospheric ^{14}C calibration curve may thus be regarded as a suite of ‘real’
217 structures, extending the calibration provided by the tree ring record for Holocene and
218 B/A-to-Early Holocene times (Fig. 2) into early deglacial and LGM times.

219

220 The plateau/jump structures may partly be linked to changes in cosmogenic ^{14}C
221 production, as possibly shown in the ^{10}Be record (Fig. 4; based on data of Adolphi et al.,
222 2018), and – presumably more dominant – to short-term changes in ocean mixing and
223 the carbon exchange between ocean and atmosphere. The exchange is crucial, since
224 the carbon reservoir of the ocean contains up to 60 (preindustrial) atmospheric carbon
225 units (Berger and Keir, 1984). The apparent contradiction with the smooth Hulu Cave
226 ^{14}C record (Southon et al., 2012; Cheng et al., 2018) may possibly be explained by the
227 Hulu Cave speleothem precipitation system acting as a low-pass filter for fluctuating
228 atmospheric ^{14}C concentrations (statistical tests of Bronk Ramsey et al., 2020) and, to a
229 very limited degree, by the obvious scatter in the Suigetsu data. The filter for Hulu data

230 possibly led to a loss especially of short-lived structures in the preserved atmospheric
231 ^{14}C record, though some remainders were preserved in the ^{14}C records of Hulu Cave
232 (Fig. 1). So we rather trust the amplitude of Suigetsu ^{14}C structures than the timing of
233 Hulu Cave data.

234

235 Like a 'rung ladder' the age-calibrated suite of ^{14}C plateau boundaries and jumps is
236 suited for tracing the calibrated age of numerous plateau boundaries in glacial-to-
237 deglacial marine ^{14}C records likewise densely sampled, even when some rungs have
238 been destroyed by local influences on gas exchange or ocean mixing. Also, one may
239 record the average offset of planktic ^{14}C ages from paired atmospheric ^{14}C ages, i.e. the
240 planktic reservoir age, for each single ^{14}C plateau (Sarnthein et al., 2007, 2015). We
241 prefer the Suigetsu record to IntCal, since it is based on original primary atmospheric
242 data and results in small-scale spatio-temporal changes of reservoir age, whereas
243 IntCal is mixing and smoothing a broad array of different data sources with comparativ-
244 ely coarse age resolution, including carbonate-based speleothem and marine records.
245 For the first time, this suite of tie points may facilitate a precise temporal correlation of
246 all sorts of changes in surface and deep-water composition on a global scale, crucial for
247 a better understanding of past changes in ocean and climate dynamics.

248

249 *1.3 Items discussed in this synthesis*

250 The Results Section is summarizing (1) Means to separate noise, global atmospheric
251 and local oceanic forcings that together control the structure of a planktic ^{14}C plateaus,
252 (2) The choice of a U/Th-based reference time scale (Bronk Ramsey et al. 2012; Cheng
253 et al., 2018) instead of the earlier varve-counted version (Schlollaut et al., 2018) to date
254 the structures in the global atmospheric ^{14}C record of Lake Suigetsu (Sarnthein et al.,

255 2015), (3) The extension of the suite of age tie points from 23 back to 29 cal. ka, values
256 crucial for an accurate global correlation of ocean events over the Last Glacial
257 Maximum, and (4) Potential linkages of atmospheric ^{14}C plateaus and jumps to
258 cosmogenic ^{14}C production and/or ocean dynamics.

259

260 The Discussion and Implications section includes:

261 (1) A global summary of published marine ^{14}C reservoir age records (Sarnthein et al.
262 2015) now enlarged by nine plateau-tuned records from the Southern Hemisphere
263 (Balmer et al., 2016 and 2018; Küssner et al., 2018 and under review) and the
264 northeast Atlantic (Ausin et al., under review). In total, 18 (LGM) / 19 (HS-1) plus three
265 wood chunk-based records (Broecker et al., 2004; Zhao et al., 2018) now depict the
266 spatio-temporal variability of past reservoir ages of surface waters in different ocean
267 regions.

268 (2) A comparison of our plateau-based reservoir ages with LGM estimates of surface
269 water ^{14}C reservoir ages simulated by the GCM of Muglia et al. (2018).

270 (3) More detailed insights into the origin of past changes in the global carbon cycle from
271 glacial to interglacial times are provided by the enlarged set of ^{14}C reservoir and venti-
272 lation ages that form a robust tracer of global circulation geometries and the inorganic
273 carbon (DIC) dissolved in different basins of the ocean (Sarnthein et al., 2013).

274

275 The discussion highlights ^{14}C plateau tuning and its revised cal. time scale for global
276 data-model intercomparison and a new understanding of Ocean MOC during the LGM
277 and its reversal during HS-1.

278

279 2. RESULTS – AGE TIE POINTS BASED ON ^{14}C PLATEAU BOUNDARIES

280

281 *2.1 Suite of planktic ¹⁴C plateaus: Means to separate global atmospheric from local*
282 *oceanographic forcings*

283 The basic assumption of the ¹⁴C plateau tuning technique is that the fine structure of
284 fluctuations of the global atmospheric ¹⁴C concentration record can also be found in the
285 surface ocean. In a plot of ¹⁴C age versus calendar age such fluctuations lead to a pattern
286 of plateaus/jumps that correspond to decreases/increases in ¹⁴C concentration. Here we
287 refer to the derivation and interpretation of planktic ¹⁴C plateaus, assuming a predom-
288 inantly global atmospheric origin with occasional local oceanographic forcings. The series
289 of planktic ¹⁴C plateaus and jumps are derived in cores with average hemipelagic
290 sedimentation rates of >10 cm/ky and dating resolution of <100-150 yr. The plateau-
291 specific structures in a sediment age-depth record form a well-defined suite for which
292 absolute age and reservoir age are derived by means of a strict alignment to the reference
293 suite of global atmospheric ¹⁴C plateaus as a whole. Initially, age tie points of planktic
294 foraminiferal $\delta^{18}\text{O}$ records showing (orbital) isotope stages #1-3 serve as stratigraphic
295 guideline for the alignment under the simplifying assumption that stratigraphic gaps are
296 absent, not always true (Suppl. Fig. 2). Planktic reservoir ages and their short-term
297 changes are derived from the difference in average ¹⁴C age between atmosphere and
298 surface waters in subsequent plateaus. To stick as close as possible to the modern range
299 of reservoir ages (Stuiver and Braziunas, 1993), tuned reservoir ages are kept at a
300 minimum unless stringent evidence requires otherwise.

301

302 A close correspondence between ¹⁴C concentrations in atmosphere and surface ocean
303 is expected based on rapid gas exchange. In several cases, however, the specific
304 structure and relative length of a planktic ¹⁴C plateau may deviate from those of the

305 pertinent plateau observed within the suite of atmospheric plateaus, thus indicate local
306 intra-plateau changes of reservoir age. Though less frequent, these changes may indeed
307 amputate and/or deform a plateau, then as result of variations in local ocean atmosphere
308 exchange and oceanic mixing. Two aspects help to sort out short-term climate-driven
309 intra- and inter-plateau changes in ^{14}C reservoir age: (i) The evaluation of the structure
310 and reservoir age of an individual plateau is strictly including the age estimates deduced
311 for the complete suite of plateaus. (ii) Our experience shows that deglacial climate
312 regimes in control of changes in surface ocean dynamics generally occurred on (multi-)
313 millennial time scales (e.g., YD, B/A, HS-1), whereas atmospheric ^{14}C plateaus hardly
314 lasted longer than a few hundred up to 1100 yr (Fig. 1 and S1). Abrupt changes in gas
315 exchange or ocean mixing usually affect one or only a few plateaus of the suite. --
316 Absolute age estimates within a plateau are derived by linear interpolation between the
317 age of the base and top of an undisturbed plateau assuming constant sedimentation
318 rates. The potential impact of short-term sedimentation pulses on ^{14}C plateau formation
319 has largely been discarded by Balmer and Sarnthein (2016).

320

321 *2.2 Suigetsu atmospheric ^{14}C record: Shift to a chronology based on U/Th model ages*

322 Originally, we based the chronology of ^{14}C plateau boundaries in the Suigetsu record
323 (Sarnthein et al., 2015) on a scheme of varve counts by means of light microscopy of
324 thin sections (Bronk Ramsey et al., 2012; Schlolaut et al., 2018). Over the crucial
325 sediment sections of the Last Glacial Maximum (LGM) and deglacial Heinrich Stadial 1
326 (HS-1), however, varve quality / perceptibility in the Suigetsu profile is highly variable
327 (Fig. 5). In parallel, varve-based age estimates were derived from counting various
328 elemental peaks in μXRF data and interpreted as seasonal signals (Marshall et al.,
329 2012). The results obtained from the two independent counting methods and their

330 interpolations widely support each other but diverge for older ages. The varve counts
331 ultimately formed the backbone of a high-resolution chronology obtained by tying the
332 Suigetsu ^{14}C record to the U/Th based time scale of the Hulu cave ^{14}C record (Bronk
333 Ramsey et al., 2012). Recently, Scholaut et al. (2018) amended the scheme of varve
334 counts. Accordingly, Suigetsu varve preservation (i.e., the number of siderite layers per
335 20 cm thick sediment section) is fairly high prior to ~32 ky BP and over late glacial
336 Termination I but fairly poor over large parts of the LGM and HS-1, from ~15 – 32 cal ka
337 (17.3-28.5 m c.d. in Fig. 5). Here only less than 20-40 % of the annual layers expected
338 from interpolation between clearly varved sections are distinguished by microscopy.
339 Varve counts that use μXRF data (Marshall et al., 2012) can distinguish subtle changes
340 in seasonal element variations, that are not distinguishable in thin section microscopy,
341 hence result in higher varve numbers especially during early deglacial-to-peak glacial
342 times. Yet, some subtle variations are difficult to distinguish from noise, which adds
343 uncertainty to the μXRF -based counts. Thus, the results from either counting method
344 are subject to uncertainties that rise with increased varve age (Fig. 5).

345

346 Bronk Ramsey et al. (2012) established a third time scale based on ^{14}C wiggle matching
347 to U/Th dated ^{14}C records of the Hulu Cave and Bahama speleothems. In part, this
348 calibrated (cal.) age scale was based on Suigetsu varve counts, in part on the
349 prerequisite of the best-possible fit of a pattern of low-frequency changes in ^{14}C
350 concentration obtained from Suigetsu and Hulu Cave. The two ^{14}C records were fitted
351 within the uncertainty envelope of the Hulu 'Old / Dead Carbon Fraction' (OCF/DCF) of
352 ^{14}C concentration. The uncertainty of this model is still incompletely understood. The
353 U/Th-based age model of Suigetsu may suffer from the wiggle matching of atmospheric
354 ^{14}C ages of Lake Suigetsu with ^{14}C ages of the Hulu Cave (Southon et al., 2012) in case

355 of major short-term changes in atmospheric ^{14}C concentration due to a memory effect of
356 soil organic carbon in carbonate-free regions of the cave overburden. The speleothem-
357 carbonate-based Hulu ages may have been influenced far more strongly by short-term
358 changes in the local DCF than assumed, as suggested by major variations in a paired
359 $\delta^{13}\text{C}$ record, that reach up to 5 ‰, mostly subsequent to short-term changes in past
360 monsoon climate (Kong et al., 2005). The uncertainty regarding the assumption of a
361 constant OCF/DCF (Southon et al. 2012; Cheng et al., 2018) may hamper the age
362 model correlation between Hulu and Suigetsu records and the Suigetsu chronology.

363

364 We compared the results of the two timescales, independently deduced from varve
365 counts, with those of the U/Th-based model age scale using as test case the base of
366 ^{14}C Plateau 2b, the oldest tie point constrained by μXRF -based counts. In contrast to
367 16.4 cal. ka, supposed by optical varve counts, μXRF -based counts suggest an age of
368 ~ 16.9 cal. ka (Marshall et al., 2012; Schlolaut et al., 2018), which matches closely the
369 U/Th-based estimate of 16.93 ka. This is a robust argument for the use of the U/Th-
370 based Suigetsu time scale as 'best possible' age scale to calibrate the age of thirty ^{14}C
371 plateau boundaries (Fig. 1). In its older part, the U/Th model time scale is further
372 corroborated by a decent match of short-term increases in ^{14}C concentration with the
373 low geomagnetic intensity of the Mono Lake and Laschamp events at ~ 34 and
374 41.1 ± 0.35 ka (Lascau et al., 2016), independently dated by other methods. The new
375 U/Th-based model ages of ^{14}C plateau boundaries are significantly higher than our
376 earlier microscopy-based varve ages over HS-1 and LGM, a difference increasing from
377 ~ 200 yr near 15.3 cal. ka to ~ 530 near 17 ka and 2000 yr near ~ 29 ka (Fig. 3).

378

379 Note, any readjustment of the calendar age of a ^{14}C plateau boundary does not entail

380 any change in ^{14}C reservoir ages afore deduced for surface waters by means of the
381 plateau technique (Sarnthein et al., 2007, 2015), since each reservoir age presents the
382 simple difference in average ^{14}C age for one and the same ^{14}C plateau likewise defined
383 in both the Suigetsu atmospheric and planktic ^{14}C records of marine surface waters,
384 independent of the precise position of this plateau on the calendar age scale.

385

386 In view of the recent revision of time scales (Schlollaut et al., 2018; Bronk Ramsey et al.,
387 2019) we now extended our plateau tuning and now also defined the boundaries and
388 age ranges of ^{14}C plateaus and jumps for the interval ~23–29 cal. ka, which results in a
389 total of ~30 atmospheric age tie points for the time span 10.5–29 cal. ka (Fig. 1;
390 summary in Table 1; following the rules of Sarnthein et al., 2007 and 2015). Prior to 25
391 cal. ka, the definition of ^{14}C plateaus somewhat suffered from an enhanced scatter of
392 raw ^{14}C values of Suigetsu. -- In addition to visual inspection, the ^{14}C jumps and
393 plateaus were also defined with higher statistical objectivity by means of the first-
394 derivative of all trends in the ^{14}C age-to-calendar age relationship (or –core depth
395 relationship, respectively) by using a running kernel window (Sarnthein et al., 2015).

396

397 *2.3 Linkages of short-term structures in the atmospheric ^{14}C record to changes in* 398 *cosmogenic ^{14}C production versus changes in ocean dynamics*

399

400 Potential sources of variability in the atmospheric ^{14}C record have first been discussed
401 by Stuiver and coworkers in the context of Holocene fluctuations deduced from tree ring
402 data (e.g., Stuiver and Braziunas 1993), more recently simulated (e.g., Hain et al.,
403 2014). -- Similar to changes in ^{14}C , variations in ^{10}Be deposition in ice cores reflect past
404 changes in ^{10}Be production as a result of changes in solar activity and the strength of

405 the Earth's magnetic field (Adolphi et al., 2018). If we accept to omit assumptions on the
406 modulation of past ^{14}C concentrations by changes in the global carbon cycle we can
407 calculate the atmospheric ^{14}C changes over last glacial-to-deglacial times with ^{10}Be and
408 a carbon cycle model and convert them into ^{14}C ages (Fig. 4). Changes in climate and
409 carbon cycle, however, over this period necessarily modified the ^{10}Be -based ^{14}C record
410 if included correctly into the modeling. Between 10 and 13.5 cal. ka, the ^{10}Be -modeled
411 ^{14}C record displays a number of plateau structures that appear to match the Suigetsu-
412 based atmospheric ^{14}C plateaus. Between 15 and 29 cal. ka, however, ^{10}Be -based ^{14}C
413 plateaus are more rare and/or less pronounced than those in the Suigetsu record. Most
414 modelled plateaus are far shorter than those displayed in the suite of atmospheric ^{14}C
415 plateaus of Lake Suigetsu (e.g., plateaus near to the top 2a, 2b, top 5a, and 9), except
416 for a distinct equivalent of plateau no. 6a. On the whole, the modelled and observed
417 structures show little coherence. This may indicate that any direct relationship between
418 variations in cosmogenic ^{14}C production and the Suigetsu plateau record is largely
419 obscured by the carbon cycle, uncorrected climate effects on the ^{10}Be deposition,
420 and/or noise in the ^{14}C data. Also, a relatively high uncertainty of the measured ^{10}Be
421 concentrations in the ice, (in many cases $\sim 7\%$; Raisbeck et al., 2017), and a lower
422 sample resolution in the order of 50 to 200 yr may contribute to the smoothed character
423 of the ^{10}Be record in Fig. 4.

424

425 On the other hand, the 'new' U/Th-based cal. ages of plateau boundaries may suggest
426 some reasonable stratigraphic correlations between peak glacial and deglacial change in
427 atmospheric CO_2 and ^{14}C plateaus with millennial-scale events in paleoceanography (Fig.
428 6, Table 2): The suite of deglacial ^{14}C plateaus no. 2a, 1, and Top YD indeed displays a
429 temporal match with three brief but major deglacial jumps in ocean degassing of CO_2

430 documented in the WDC ice core (Marcott et al., 2014). The two records have been
431 independently dated by means of annual-layer counts in ice cores and U/Th ages of
432 stalagmites. The match suggests that these atmospheric ^{14}C plateaus may largely result
433 from changes in air-sea gas exchange, and in turn, from changes in ocean dynamics.

434

435 In particular, these events may have been linked to a variety of fast changes such as in
436 sea ice cover in the Southern Ocean and/or in the salinity and buoyancy of high-latitude
437 surface waters (Skinner et al., 2010; Burke and Robinson, 2012). These factors control
438 upwelling and meridional overturning of deep waters, in particular found in the Southern
439 Ocean (Chen et al., 2015) and/or North Pacific (Rae et al. 2014, Gebhardt et al., 2008).
440 Such events of changes in MOC geometry and intensity may be responsible for ocean
441 degassing and the ^{14}C plateaus. The enhanced mixing of the Southern Ocean and a
442 similar, slightly later mixing event in the North Pacific (MD02-2489; Fig. S2d) may have
443 triggered – with phase lag – two trends in parallel, (1) a rise in atmospheric CO_2 , in part
444 abrupt (*sensu* Chen et al., 2015; Menviel et al., 2018), and (2) a gradual enrichment in ^{14}C
445 depleted atmospheric carbon, reflected as ^{14}C plateau.

446

447 Plateau 6a matches a ^{14}C plateau deduced from atmospheric ^{10}Be concentrations, thus
448 suggests changes in ^{14}C production. Other changes in atmospheric ^{14}C (plateaus 4 and
449 8) match short-term North Atlantic warmings during peak glacial and earliest deglacial
450 times, similar to that at the end of HS-1 and during plateau 'YD', hence may reflect
451 minor changes in ocean circulation and ocean-atmosphere exchange without major
452 degassing of old ^{14}C depleted deep waters in the North Atlantic (Table 2, Fig. S2a).

453 There is still little information, however, on the origin of several other peak glacial ^{14}C

454 plateaus 17.5–29 cal. ka. The actual linkages of these plateaus to events in ocean MOC
455 still remain to be uncovered.

456

457 3. DISCUSSION and IMPLICATIONS

458 *3.1 ¹⁴C plateau boundaries – A suite of narrow-spaced age tie points to rate short-term*
459 *changes in marine sediment budgets, chemical inventories, and climate 29–10 cal. ka*

460

461 In continuation of previous efforts (Sarthein et al., 2007 and 2015) the tuning of high-
462 resolution planktic ¹⁴C records of ocean sediment cores to the new age-calibrated
463 atmospheric ¹⁴C plateau boundaries now makes it possible to establish a ‘rung ladder’
464 of ~30 age tie points covering the time span 29 – 10 cal. ka. These global tie points
465 have a time resolution of several hundred to thousand years to be used to constrain the
466 chronology and potential leads and lags of events that occurred during peak glacial and
467 deglacial times (Fig. 1). The locations of 18 (20; depending on the age range covered)
468 ¹⁴C records are shown in Fig. 7. Figs. 8 and S2 give the time histories of the planktic
469 and benthic reservoir ages, the information they provide is discussed below.

470

471 Six prominent examples showing the power and value of additional information obtained
472 by means of the ¹⁴C plateau-tuning method are:

473 (i) The timing of ocean signals of the onset of deglaciation (sudden depletion of
474 planktic $\delta^{18}\text{O}$ and rise in SST) in the North Atlantic and North Pacific can now be
475 distinguished in detail from those in the Southern Hemisphere, where warming began at
476 17.6 cal. ka, when the cooling of Heinrich 1 started in the North Atlantic (Fig. S2)
477 (Küssner et al., under review); in harmony with Schmittner and Lund, 2015), a finding
478 important to further constrain global ‘bipolar see-saw’ (Stocker and Johnsen, 2003).

479 (ii) Likewise, the end of the cooling equated with the Antarctic Cold Reversal (ACR;
480 WDC Project Members, 2013) in Pacific surface waters off Central Chile was found
481 precisely coeval with the onset of the Younger Dryas cold spell in the Northern
482 Hemisphere (Küssner et al., under review).

483 (iii) Signals of local deep-water formation in the subpolar North Pacific can now be
484 separated from signals originating in the North Atlantic (Rae et al. 2014; Sarnthein et al.,
485 2013). In this way we now can specify and tie major short-lasting reversals in Atlantic
486 and Pacific MOC on a global scale.

487 (iv) Signals of deglacial meltwater advection can now be distinguished from short-
488 term interstadial warmings in the northern subtropical Atlantic, which helps to locate
489 meltwater outbreaks far beyond the well-known Heinrich belt of ice-rafted debris
490 (Balmer and Sarnthein, 2018).

491 (v) As outlined above, the timing of marine ^{14}C plateaus can now be compared in
492 detail with that of deglacial events of climate and the atmospheric CO_2 rise independ-
493 ently dated by means of ice core-based stratigraphy (Table 2; Fig. 6). These linkages
494 offer a tool to explore details of deglacial changes in deep-ocean MOC once the suite of
495 ^{14}C plateaus has been properly tuned at any particular ocean site.

496 (vi) The refined scale of age tie points also reveals unexpected details for changes in
497 the sea ice cover of high latitudes as reflected by anomalously high ^{14}C reservoir ages
498 (e.g. north of Iceland and near to the Azores Islands) and for the evolution of Asian
499 summer monsoon in the northern and southern hemisphere as reflected by periods of
500 reduced sea surface salinity (e.g., Sarnthein et al., 2015; Balmer et al., 2018).

501

502 Finally, the plateau-based high-resolution chronology has led to the detection of
503 numerous millennial-scale hiatuses (e.g., Sarnthein et al., 2015; Balmer et al., 2016;

504 Küssner et al., under review) overlooked by conventional, e.g., *AnalySerie*-based
505 methods (Paillard et al. 1996) of stratigraphic correlation (Fig. S2). In turn, the hiatuses
506 give intriguing new insights into past changes of bottom current dynamics linked to
507 different millennial-scale geometries of overturning circulation and climate change such
508 as in the South China Sea (Sarnthein et al., 2013 and 2015), in the South Atlantic
509 (Balmer et al. 2016) and southern South Pacific (Ronge et al., 2019).

510

511 Clearly, the new atmospheric ^{14}C 'rung ladder' of closely-spaced chronostratigraphic tie
512 points has evolved to a valuable tool to uncover functional chains in paleoceanography,
513 that actually have controlled events of climate change over glacial-to-deglacial times.
514 The extension of the age range back to 29 ka allows constraining potential changes in
515 the ocean dynamics expected for Dansgaard Oeschger (DO) events 2, 3, and 4 as
516 compared to those found for DO-1, though pertinent core records are still missing.

517

518 *3.2 Observed vs. model-based ^{14}C reservoir ages that act as tracer of past changes in*
519 *surface ocean dynamics provide incentive for model refinements*

520

521 Radiocarbon plateau tuning of marine sediment sections to the Suigetsu ^{14}C
522 atmospheric master record allows us to establish at semi-millennial-scale resolution the
523 difference between the average ^{14}C age of coeval atmospheric and planktic ^{14}C
524 plateaus. The suite of changing ^{14}C reservoir ages over time forms a prime tracer of
525 past ocean dynamics influencing local surface waters and a data set crucial to deduce
526 past apparent deep-water ventilation ages (e.g., Muglia et al., 2018; Cook and Keigwin,
527 2015; Balmer and Sarnthein, 2018).

528

529 To better constrain the water depth of past reservoir ages we dated monospecific
530 planktic foraminifera (Sarnthein et al., 2007); in low-to-mid latitudes on *G. bulloides*, *G.*
531 *ruber*, or *G. sacculifer* with habitat depths of 0–80/120 m (Jonkers and Kucera, 2017)
532 and in high latitudes, mostly on *N. pachyderma* (s) living at 0–200 m depth (Simstich et
533 al., 2003). Averaging of ^{14}C ages within a ^{14}C plateau helps to remove analytical noise
534 and minor real ^{14}C fluctuations. Nine plateaus are located in the LGM, 18–27 cal. ka
535 (Fig. 1). Here, planktic foraminifera-based reservoir ages show analytical uncertainties
536 of >200 to >300 yr each for standard AMS dating. By comparison, short-term temporal
537 variations in reservoir age reach 200–400 yr, occasionally up to 600 yr, in particular,
538 close to the end of the LGM (Table 3).

539

540 To better decode the informative value of our ^{14}C reservoir ages for late LGM we
541 compared average ages of ^{14}C Plateaus 4-5 (18.6–20.9 cal. ka) with estimates
542 generated by various global ocean models, an approach similar to that of Toggweiler et
543 al. (2019) applied to modern reservoir ages of the global ocean. In an earlier paper
544 (Balmer et al., 2016) we compared our empiric reservoir ages for the LGM with GCM-
545 based estimates of Franke et al. (2008) and Butzin et al. (2012). Franke et al. (2008)
546 underestimated our mid-latitude values by up to ~2000 ^{14}C yr, while LGM reservoir age
547 estimates of Butzin et al. (2012) were more consistent with ours. Their GCM
548 considered more realistic boundary conditions such as the LGM freshwater balance in
549 the Southern Ocean and, in particular, LGM SST and wind fields plus the gas transfer
550 velocity for the exchange of ^{14}C of CO_2 (Sweeney et al., 2007). Further improvements
551 are expected from a model configuration that properly resolves the topographic details
552 of the continental margins and adjacent seas, which frequently form the origin of our
553 sediment-based data sets (Butzin et al., 2020). For the time being, we compared our

554 empirical estimates with estimates from a coarse-resolution GCM, using the results by
555 Muglia et al. (2018; 0–50 m w.d.; Fig. 8c-d; Table 3) as an example. Their model
556 includes ocean surface reservoir age and ocean radiocarbon fields that have been
557 validated through a comparison to LGM ^{14}C data compilation made by Skinner et al.
558 2017. It conforms two plausible, recent model estimates of surface reservoir ages that
559 can be compared to our results (Table 3).

560

561 Low LGM values (300–750 yr) supposedly document an intensive exchange of surface
562 waters with atmospheric CO_2 , most common in model- and foraminifera-based
563 estimates of the low- and mid-latitude Atlantic. Low empiric values also mark LGM
564 waters in mid to high latitudes off Norway and off middle Chile, that is, close to sites of
565 potential deep and/or intermediate water formation. Off Norway and in the northeastern
566 Atlantic, model-based reservoir ages of Muglia et al. (2018) largely match the empiric
567 range. However, the uncertainty envelopes for data shown in Fig. 8c (± 560 yr; $r = 0.59$)
568 generally exceed by far the spatial differences calculated for the empiric data.
569 Conversely, model-based reservoir ages reproduce only poorly the low planktic
570 foraminifera-based estimates off Central Chile and values in the Western Pacific and
571 Southern Ocean.

572 In part, the differences may be linked to problems like insufficient spatial resolution
573 along continental margins, ignoring east-west differences within ocean basins, and/or
574 the estimates of a correct location and extent of seasonal sea ice cover used as LGM
575 boundary condition such as east off Greenland, in the subpolar northwest Pacific, and
576 off Southern Chile, where sea ice hindered the exchange of atmospheric carbon (per
577 analogy to that of temperature exchange, e.g., Sessford et al, 2019). Also, model
578 estimates of the annual average are compared to ^{14}C signals of planktic foraminifera

579 that mostly formed during summer only, e.g., when large parts of the Nordic Seas were
580 found ice-free (Sarnthein et al., 2003). Hence, models may need to better constrain
581 local and seasonal sealing effects of LGM sea ice cover.

582

583 In general, the foraminifera-based reservoir age estimates for our sites that represent
584 various hydrographic key regions in the high-latitude ocean appear much higher than
585 model-derived values. These deviations reach up to 1400 yr, in particular in the
586 Southern Ocean. In part, they may result from the fact that present models may not yet
587 be suited to capture small-scale ocean structures such as the interference of ocean
588 currents with local bathymetry and local upwelling cells. Here, model-based reservoir
589 ages appear far too low in LGM regions influenced by regional upwelling such as the
590 South China Sea then governed by an estuarine overturning system (Wang et al., 2005;
591 Fig. 9), by coastal upwelling off N.W. Australia (Xu et al., 2010; Sarnthein et al., 2011),
592 or by a melt water lid such as off eastern New Zealand (Bostock et al., 2013; Küssner et
593 al., under review). Local oceanic features are likely to be missed in current resolution
594 models. Our more narrow-spaced empiric data could help to refine the skill of models to
595 capture past ^{14}C reservoir ages.

596

597 Various differences amongst plankton- and model-based reservoir ages may also result
598 from differential seasonal habitats of the different planktic species analyzed that, in turn,
599 may trace different surface and subsurface water currents. Distinct interspecies
600 differences were found in Baja California that record differential, upwelling-controlled
601 habitat conditions (Lindsay et al, 2015). In the northern Norwegian Sea interspecies
602 differences amount up to 600 yr for the Preboreal ^{14}C plateau, 9.6–10.2 cal. ka
603 (Sarnthein and Werner, 2018). Here ^{14}C records of Arctic *Turborotalita quinqueloba*,

604 dominantly grown close to the sea surface during peak summer, differ from the paired
605 record of *Neogloboquadrina pachyderma*, formed in subsurface waters, and that of
606 subpolar species *N. incompta*, mainly advected from the south by Norwegian Current
607 waters well mixed with the atmosphere during peak winter. This makes closer
608 specification of model results as product of different seasonal extremes a further target.
609

610 3.3 Planktic foraminifera-based ^{14}C reservoir ages – A prime database to estimate past 611 changes in the ^{14}C ventilation age of deep waters and past oceanic MOC and DIC 612

613 ‘Raw’ apparent benthic ventilation ages (in ^{14}C yr; ‘raw’ *sensu* Balmer et al., 2018)
614 express the difference between the (coeval) atmospheric and benthic ^{14}C levels
615 measured at any site and time of foraminifer deposition. These ages are the sum of (1)
616 the planktic reservoir age of the ^{14}C plateau that covers a group of paired benthic and
617 planktic ^{14}C ages and (2) the (positive or negative) ^{14}C age difference between any
618 benthic ^{14}C age and the average ^{14}C age of the paired planktic ^{14}C plateau. The benthic
619 ventilation ages necessarily rely on the high quality of ^{14}C plateau-based chronology,
620 since the atmospheric ^{14}C level has been subject to substantial short-term changes over
621 glacial-to-deglacial times. Necessarily, the ventilation ages include a mixing of different
622 water masses that might originate from different ocean regions and may contribute
623 differential ^{14}C ventilation ages, an unknown justifying the modifier ‘apparent’.

624

625 In a further step, the $\Delta\Delta^{14}\text{C}$ equivalent of our ‘raw’ benthic ventilation age may be
626 adjusted to changes in atmospheric ^{14}C that occurred over the (short) time span
627 between deep-water formation and benthic sediment deposition (e.g., Balmer and
628 Sarnthein, 2018; Cook and Keigwin, 2015). In most cases, however, this second step is

629 omitted since its application usually does not imply any major modification of the
630 ventilation age estimates (Fig. S2a; Skinner et al., 2017; Sarnthein et al., 2013).

631

632 On the basis of ^{14}C plateau tuning we now can rely on 18 accurately dated records of
633 apparent benthic ^{14}C ventilation ages (Fig. S2a-d) to reconstruct the global geometry of
634 LGM and HS-1 deep and intermediate water circulation as summarized in ocean
635 transects and maps (Figs. 9–11) and discussed below. The individual matching of our
636 20 planktic ^{14}C plateau sequences with that of the Suigetsu atmospheric ^{14}C record is
637 displayed in Sarnthein et al. (2015), Balmer et al., (2016), Küssner et al. (under review),
638 and Ausin et al. (under review). In addition, robust estimates of past reservoir ages are
639 obtained for 4 planktic and benthic ^{14}C records from paired atmospheric ^{14}C ages of
640 wood chunks (Rafter et al., 2018; Zhao and Keigwin, 2018; Broecker et al., 2004).

641

642 *3.3.1 — Major features of ocean meridional overturning circulation during LGM (Fig. 10)*

643

644 Off Norway and near the Azores Islands very low benthic ^{14}C ventilation ages of <100–
645 750 yr suggest ongoing deep-water formation in the LGM northern North Atlantic
646 reaching down to more than 3000–3500 m water depth, with a flow strength possibly
647 similar to today (and a coeval deep countercurrent of old waters from the Southern
648 Ocean flowing along the East Atlantic continental margin off Portugal). This pattern
649 clearly corroborates the assembled benthic $\delta^{13}\text{C}$ record showing plenty of elevated $\delta^{13}\text{C}$
650 values for the northwestern, eastern and central North Atlantic (Sarnthein et al., 1994;
651 Millo et al., 2006; Keigwin and Swift, 2017). Irrespective of unspecified potential zonal
652 variations in deep-water ventilation age at mid latitudes and different from a number of
653 published models (e.g., Ferrari et al., 2014; Butzin et al., 2017) this ‘anti-estuarine’

654 pattern has been confirmed by a global tracer transport model of Gebbie (2014),
655 MIROC model simulations (Sherriff-Tadano et al., 2017, Yamamoto et al., 2019), and
656 independently, by ϵ_{Nd} records (Howe et al., 2016; Lippold et al., 2016). The latter
657 suggest an overturning of AMOC possibly even stronger than today, in particular due to
658 a 'thermal threshold' (Abé-Ouchi, 2018) overlooked in other model simulations.

659

660 In contrast to the northern North Atlantic, deep waters in the southern North Atlantic and
661 Circumpolar (CP) deep waters in the subpolar South Atlantic show an LGM ^{14}C
662 ventilation age of ~3640 yr, finally rising up to 3800 yr (Figs. 10, 11, S2b). These waters
663 were upwelled and admixed from below to surface waters near to the sub-Antarctic
664 Front during terminal LGM (Fig. S2b; Skinner et al., 2010; Balmer and Sarnthein, 2016;
665 model of Butzin et al., 2012).

666

667 In the southwestern South Pacific abyssal, in part possibly Antarctic-sourced waters
668 (Rae and Broecker, 2018) likewise show high apparent ^{14}C ventilation ages of 3500 yr
669 that drop to 2750 yr near the end of the LGM (Figs. 10 top and S2c) (^{14}C dates of
670 Ronge et al., 2016, modified by planktic ^{14}C reservoir ages of Küssner et al., under
671 review). A vertical transect of benthic $\delta^{13}C$ (McCave et al., 2008) suggests that the
672 abyssal waters were overlain by CP waters, separated by pronounced stratification near
673 ~3500–4000 m water depth. In part, the CP waters stemmed from North Atlantic Deep
674 Water. Probably, their apparent ventilation age 3500 yr came close to the values found
675 in the southern South Atlantic. East of New Zealand the CP waters entered the deep
676 western Pacific and spread up to the subpolar North Pacific, where LGM ^{14}C ventilation
677 ages reached ~3700 yr, possibly occasionally 5000 yr (Fig. S2d).

678

679 Similar to today, the MOC of the LGM Pacific was shaped by estuarine geometry,
680 probably more weakened than today (Du et al., 2018) and more distinct in the far
681 northwest than in the far northeast. This geometry resulted in an upwelling of old deep
682 waters in the subarctic Northwest Pacific, here leading to a ^{14}C reservoir age of ~1700
683 yr for surface waters at terminal LGM. On top of the Lower Pacific Deep Waters we may
684 surmise Upper Pacific Deep Waters that moved toward south (Figs. 10 top and 11).

685

686 The Pacific deep waters were overlain by Antarctic / Pacific Intermediate Waters (IW)
687 with LGM ^{14}C ventilation ages as low as 1400–1800 yr, except for a shelf ice-covered
688 site at the southern tip of Chile with IW ages of 2400–2900 yr, possibly a result of local
689 upwelling of CP waters. In general, however, the low values of Pacific IW are similar to
690 those estimated for South Atlantic IW and likewise reflect a vivid exchange with
691 atmospheric CO_2 in their source regions in the Southern Ocean (Skinner et al., 2015).

692

693 When entering and crossing the entrance sill to the marginal South China Sea the
694 ‘young’ IW were mixed with ‘old’ CP waters entrained from below, here leading to ^{14}C
695 ventilation ages of 2600–3450 yr (Figs. 9 and S2d). The LGM South China Sea was
696 shaped by an estuarine-style overturning system marked by major upwelling near to its
697 distal end in the far southwest (Wang L. et al., 1999). This upwelling led to planktic ^{14}C
698 reservoir ages as high as 1200–1800 yr, values rarely found elsewhere in surface
699 waters of low latitudes.

700

701 Our wide-spaced distribution pattern of 18 open-ocean ^{14}C ventilation ages (plus 4
702 values based on paired wood chunks) in Figs. 10 and 11 agrees only in part with the
703 circulation patterns suggested by the much larger datasets of ^{14}C ventilation ages

704 compiled by Skinner et al. (2017) and Zhao et al. (2018). Several features in Figs. 10
705 and 11 directly deviate, e.g., the ages we derive for the North Atlantic and mid-depth
706 Pacific. These deviations may be linked to both the different derivation of our ^{14}C
707 ventilation age estimates and the details of our calendar-year chronology now based on
708 the narrow-standing suite of ^{14}C plateau-boundary ages. The quality of our ^{14}C reservoir
709 ages of surface waters also controls the 'apparent' ventilation age of deep-waters, as it
710 results from direct addition of the short-term average ^{14}C age of a planktic ^{14}C plateau to
711 a paired, that is coeval benthic ^{14}C age (formed during the time of benthic foraminiferal
712 growth, somewhat after the actual time of deep-water formation).

713

714 *3.3.2 — Major features of meridional overturning circulation during early HS-1 (Fig. 10)*

715

716 Near the onset of deglacial Heinrich Stadial 1 (HS-1; ~18–14.7 cal. ka) major shifts in
717 ^{14}C ventilation age suggest some short-lasting but fundamental changes in the
718 circulation geometry of the deep ocean, a central theme of marine paleoclimate
719 research (lower panel of Figs. 10, 11 and S2a and b). Deep waters in the eastern
720 Nordic Seas, west of the Azores Islands, and off northern Brazil show a rapid rise to
721 high ^{14}C ventilation ages of ~2000–2500 yr and up to 4000 yr off Brazil, values that give
722 first proof for a brief switch from 'anti-estuarine' to 'estuarine' circulation that governed
723 the central North Atlantic and Norwegian Sea during early HS-1. This geometry
724 continued – except for a brief but marked and widespread event of recurring NADW
725 formation near 15.2 ka – until the very end of HS-1 near 14.5 ka (Fig. S2a; Muschitiello
726 et al., 2019). The MOC switch from LGM to HS-1 is in line with changes depicted in
727 paired benthic $\delta^{13}\text{C}$ data (Sarnthein et al., 1994), but not confirmed by the coeval ϵ_{Nd}

728 record that suggests a constant source of ‘mid-depth waters’, with the $\delta^{13}\text{C}$ drop being
729 simply linked to a higher age (Howe et al., 2018).

730

731 Conversely, benthic ^{14}C ventilation ages in the northeastern North Pacific (Site MD02-
732 2489) show a coeval and distinct but brief minimum of 1050-1450 yr near 3640 m w.d.
733 during early HS-1 (~18.1–16.8 ka; Figs. 10, 11, and S2d). This minimum was produced
734 by extremely small benthic-planktic age differences of 350–650 yr and provides robust
735 evidence for a millennial-scale event of deep-water formation, that has flushed the
736 northeastern North Pacific down to more than 3640 m w.d. (Gebhardt et al., 2008;
737 Sarnthein et al., 2013; Rae et al., 2014). Similar circulation geometries were reported for
738 the Pliocene (Burls et al., 2017). ‘Young’ Upper North Pacific Deep Waters (North
739 Pacific Intermediate Waters *sensu* Gong et al., 2019) then penetrated as ‘western
740 boundary current’ far south, up to the northern continental margin of the South China
741 Sea (Figs. 9b, 11, and S2d). The short-lasting North Pacific regime of anti-estuarine
742 overturning was similar to that we find in the modern and LGM Atlantic and, most
743 interesting, simultaneous with the Atlantic's estuarine episode.

744

745 Recent data on benthic-planktic ^{14}C age differences (Du et al., 2018) precisely recover
746 our results in a core at ~680 m w.d. off southern Alaska. However, they do not depict
747 the ‘young’ deep waters at their Site U1418 at ~3680 m w.d., as corroborated by a
748 paired autigenic ϵ_{Nd} maximum suggesting a high local bottom water age nearby. We
749 assume that the amazing difference in local deep-water ventilation ages is due to small-
750 scale differences in the effect of Coriolis forcing at high latitudes between a site located
751 directly at the base of the Alaskan continental margin (U1418; Fig. 10b) and that on the
752 distal Murray Sea Mount in the ‘open’ Pacific (MD02-2489; Figs. 7 and 11), which

753 probably has been washed by a plume of newly formed North Pacific deep waters
754 probably stemming from the Bering and/or Ochotsk Seas. In contrast, the incursion of
755 almost 3000 yr old deep waters from the Southern Ocean has continued along the
756 continental margin all over HS-1. In summary we may conclude that the geometry of
757 ocean MOC was briefly reversed in the 'open' North Pacific over almost 1500 years
758 during HS-1, far deeper than suggested by previous authors (e.g., Okazaki et al., 2012;
759 Gong, S., et al. 2019), but similar to changes in geometry first proposed by Broecker et
760 al. (1985) then, however, for an LGM ocean.

761

762 3.3.3 — *Deep-Ocean DIC inventory*

763

764 Apart from the changing geometries in ocean MOC during LGM and HS-1, the global
765 set of ^{14}C plateau-based, hence refined estimates of apparent ^{14}C ventilation ages (Fig.
766 10) has ultimately also revealed new insights into glacial-to-deglacial changes in deep-
767 ocean DIC inventories (Sarnthein et al., 2013; Skinner et al., 2019). On the basis of
768 GLODAP data (Key et al., 2004) any drop in ^{14}C concentration (i.e., any rise in average
769 ^{14}C ventilation age) of modern deep waters is tied linearly to a rise of carbon (DIC)
770 dissolved in deep ocean waters below ~2000 m, making for 1.22 micromole C / -1 ‰
771 ^{14}C . By and large, GCM and box model simulations of Chikamoto and Abé-Ouchi (2012)
772 and Wallmann et al. (2016) suggest that this ratio may also apply to LGM deep-water
773 circulation, when apparent ^{14}C ventilation ages in the Southern Ocean increased
774 significantly (from 2400 up to ~3800 yr) and accordingly, thermohaline circulation was
775 more sluggish and transit times of deep waters extended. Accordingly, a 'back-of-the-
776 envelope' calculation of LGM ventilation age averages in the global deep ocean
777 suggests an additional carbon absorption of 730–980 Gt (Sarnthein et al., 2013). This

778 estimate can easily accommodate the glacial transfer of ~200 Gt C from the atmosphere
779 and biosphere, moreover, may also explain 200–450 Gt C then most probably removed
780 from glacial Atlantic and Pacific intermediate waters. These estimates offer an
781 independent evaluation of ice core-based data, other proxies, and model-based data on
782 past changes in the global carbon cycle (e.g., Menviel et al., 2018).

783

784 4. SOME CONCLUSIONS AND PERSPECTIVES

785 – Despite some analytical scatter, ^{14}C ages for the top and base of Lake Suigetsu-
786 based atmospheric ^{14}C plateaus and coeval planktic ^{14}C plateaus do not present
787 statistical ‘outliers’ but real age estimates that are reproduced by tree ring-based ^{14}C
788 ages over the interval 10–13 cal. ka and further back.

789 – Hulu U/Th model-based ages of ^{14}C plateau boundaries of the Suigetsu atmospheric
790 ^{14}C record appear superior to those derived from microscopy-based varve counts only,
791 since U/Th model-based ages match far more closely the age when now deduced from
792 XRF-based varve counts for the tie point of lower plateau boundary 2b, a test case in
793 the early deglacial, and for the age assigned to the Laschamp event prior to the LGM.

794 – During deglacial times, we show that several atmospheric ^{14}C plateaus paralleled a
795 rise in air-sea gas exchange, and, in turn, distinct changes in ocean MOC. Changes in
796 cosmogenic ^{14}C production rarely provide a complete explanation for the plateaus
797 identified in the Suigetsu ^{14}C data under discussion.

798 – In total, ^{14}C plateau boundaries in the range now provide a suite of ~30 age tie points
799 to establish – like chronological ladder rungs – a robust global age control for deep-sea
800 sediment sections and global stratigraphic correlations of last glacial to deglacial climate
801 events, 29–10 cal. ka. U/Th model ages confine the cal. age uncertainty of Suigetsu
802 plateau boundaries assigned halfway between two ^{14}C ages nearby inside and outside

803 a plateau's scatter band to less than ± 50 to ± 70 yr. Nevertheless, stratigraphic gaps
804 may hamper the accurate tuning of planktic ^{14}C plateaus to their atmospheric
805 equivalents hence result in major discrepancies.

806 – The difference in ^{14}C age between coeval atmospheric and planktic ^{14}C plateaus
807 presents a robust tracer of planktic ^{14}C reservoir ages and shows their high temporal
808 and spatial variability for the LGM and HS-1, now established for 18/20 sediment sites.

809 – Paired reservoir ages obtained from different planktic species document the local
810 distribution patterns of different surface water masses and prevailing foraminiferal
811 habitats at different seasons yet insufficiently considered in model simulations.

812 – New, more robust deep-water ^{14}C ventilation ages, derived on the basis of our robust
813 planktic ^{14}C reservoir ages, reveal geometries of LGM overturning circulation similar to
814 those of today. In contrast, ^{14}C ventilation ages of early HS-1 suggest an almost 1500 yr
815 long event of widely reversed circulation patterns marked by deep-water formation and
816 brief flushing of the northern North Pacific and estuarine circulation geometry in the
817 northern North Atlantic.

818 – Increased glacial ^{14}C ventilation ages and carbon (DIC) inventories of ocean deep
819 waters suggest an LGM drawdown of about 850 Gt C into the deep ocean. Starting with
820 HS-1 a drop of ventilation age suggests carbon released to the atmosphere (Sarnthein
821 et al., 2013).

822 – Site-specific comparison of planktic and model-based reservoir ages estimates
823 highlights the need for further model refinements to make them better reflect the real
824 complex patterns of ocean circulation, including seasonality.

825

826 ACKNOWLEDGMENTS

827 We owe sincere thanks for plenty of stimulations to the 23rd International Radiocarbon
828 Conference in Trondheim, in particular to M-J. Nadeau, and to the IPODS–OC3
829 workshop in Cambridge U.K, 2018, convened by A. Schmittner and L. Skinner.
830 Moreover, we thank for most valuable basic discussions with R. Staff, Glasgow, J.
831 Southon, Irvine CA, and M. Butzin, AWI Bremerhaven, who kindly helped us to discuss
832 the comparison of his model results, and S. Beil, Kiel, for computer assistance. Over the
833 last three years, G. Mollenhauer measured with care hundreds of supplementary ¹⁴C
834 ages in her MICADAS laboratory at AWI Bremerhaven. This study obtained long lasting
835 special support from R. Tiedemann and his colleagues at the AWI Bremerhaven.

836

837 **Author contribution**

838 All authors contributed data and valuable suggestions to write up this synthesis. MS and
839 PG designed the outline of this manuscript. KK, BA, TE and MS provided new marine
840 ¹⁴C records in addition to records previously published. GS displayed the details of
841 Suigetsu varve counts. RM provided a ¹⁰Be-based ¹⁴C record and plots of raw ¹⁴C data
842 sets of Suigetsu und Hulu Cave. Discussions amongst PG, RM, GS and MS served to
843 select U/Th-based model ages as best-possible time scale. JM streamlined the sections
844 on data-model intercomparison.

845

846 **Data availability**

847 Published primary radiocarbon data of all sites are available at PANGAEA de. ¹⁴C data
848 of five marine sediment cores still under publication by Küssner et al. (under review)
849 and Ausin et al. (under review; also see caption of Fig. S2) are deposited at
850 PANGAEA® under <https://doi.org/10.1594/PANGAEA.922671> and

851 <https://doi.org/10.1594/PANGAEA.921812>

852

853

854

855

856 REFERENCES

- 857 Abé-Ouchi, A.: Deglaciation and DO-like experiments with MIROC AOGCM.
858 Abstract, IPODS/OC3 -Workshop on 'Ocean circulation and carbon cycling during the
859 last deglaciation: Global synthesis'. Cambridge 2018.
- 860 Adkins, J. F. and Boyle, E. A.: Changing atmospheric $\Delta^{14}\text{C}$ and the record of
861 paleoventilation ages. *Paleoceanography*, 12(3), 337–344, 1997.
- 862 Adolphi, F., Bronk Ramsey, C., Erhard, T., Lawrence Edwards, R., Cheng, H.,
863 Turney, C.S.M., Cooper, A., Svensson, A., Rasmussen, S.O., Fischer, H., and
864 Muscheler, R.: Connecting the Greenland ice-core and U/Th timescales via cosmogenic
865 radionuclides: testing the synchronicity of Dansgaard–Oeschger events. *Clim. Past*, 14,
866 1755–1781. <https://doi.org/10.5194/cp-14-1755-2018>, 2018.
- 867 Alves, E.Q., Macario, K., Ascough, P., and Bronk Ramsey, C.: The worldwide
868 marine radiocarbon reservoir effect: definitions, mechanisms, and prospects. *Review of*
869 *Geophysics*, 56, <https://doi.org/10.1002/2017RG000588>, 2018.
- 870 Alveson, E.Q.: Radiocarbon in the Ocean, *EOS*, 99,
871 <https://doi.org/10.1029/2018EO095429>, 2018.
- 872 Ausin, B., Haghypour, N., Wacker, L., Voelker, A. H. L., Hodell, D., Magill, C., et al.:
873 Radiocarbon age offsets between two surface dwelling planktonic foraminifera species
874 during abrupt climate events in the SW Iberian margin. *Paleoceanography and*
875 *Paleoclimatology*, 34. <https://doi.org/10.1029/2018PA003490>, 2019.
- 876 Ausin, B., Sarnthein, M., and Haghypour, N.: Glacial-to-deglacial reservoir and
877 ventilation ages at the southwest Iberian continental margin. *Quaternary Science*
878 *Reviews* (under review).
- 879 Balmer, S., Sarnthein, M., Mudelsee, M., and Grootes, P. M.: Refined modeling and
880 ^{14}C plateau tuning reveal consistent patterns of glacial and deglacial ^{14}C reservoir ages
881 of surface waters in low-latitude Atlantic. *Paleoceanography*, 31.
882 <https://doi.org/10.1002/2016PA002953>, 2016.
- 883 Balmer, S. and Sarnthein, M.: Planktic ^{14}C plateaus, a result of short-term
884 sedimentation pulses? – *Radiocarbon*, 58, DOI:10.1017/RDC.2016.100, 11 pp., 2016.
- 885 Balmer, S. and Sarnthein, M.: Glacial-to deglacial changes in North Atlantic melt-
886 water advection and deep-water formation – Centennial-to-millennial-scale ^{14}C records
887 from the Azores Plateau. *Geochim. Cosmochim. Acta*, 236, 399-415,
888 <https://doi.org/10.1016/j.gca.2018.03.001>, 2018.

889 Berger W.H. and Keir, R.S.: Glacial-Holocene changes in atmospheric CO₂ and the
890 deep-sea record. J.E. Hansen, T. Takahashi (Eds.), Geophysical Monograph, 29,
891 American Geophysical Union, Washington, DC, pp. 337–351, 1984.

892 Bostock, H.C., Barrows, T.T., Carter, L., Chase, Z., Cortese, G., et al.: A review of
893 the Australian – New Zealand sector of the Southern Ocean over the last 30 ka (Aus-
894 INTIMATE project). *Quaternary Science Reviews* 74, 35-57, 2013.

895 Broecker W.S, Peteet, D.M., and Rind, D.: Does the ocean-atmosphere system have
896 more than one stable mode of operation? *Nature*, **315**, 21-26, doi:10.1038/315021a0,
897 1985

898 Broecker W.S., Barker, S., Clark, E., Hajdas, I., Bonani, G., and Stott, L.: Ventilation
899 of the Glacial deep Pacific Ocean, *Science*, 306, 1169–1172, 2004.

900 Bronk Ramsey, C., Staff, R. A., Bryant, C. L., Brock, F., Kitagawa, H., van der Plicht,
901 J., Scholaut, G., Marshall, M. H., Brauer, A., Lamb, H. F., Payne, R. L., Tarasov, P. E.,
902 Haraguchi, T., Gotanda, K., Yonenobu, H., Yokoyama, Y., Tada, R., and Nakagawa, T.:
903 A complete terrestrial radiocarbon record for 11.2 to 52.8 kyr B.P., *Science*, 338, 370–
904 374, 2012.

905 Bronk Ramsey, C., Heaton, T.J., Scholaut, G., Staff, R.A., Bryant, C.L., Lamb, H.F.,
906 Marshall, M.H., Nakagawa, T.: Reanalysis of the atmospheric radiocarbon calibration
907 record from Lake Suigetsu, Japan. *Radiocarbon*, <https://doi.org/10.1017/RDC.2020.18>,
908 2020

909 Burke, A. and Robinson, L.F.: The Southern Ocean's role in carbon exchange during
910 the last deglaciation. *Science*, 335, 557-561, 2012.

911 Burls, N.J., Fedorov, A.V., Sigman, D.M., Jaccard, S.L., Tiedemann, R., and Haug,
912 G.H.: Active Pacific meridional overturning circulation (PMOC) during the warm
913 Pliocene. *Sci. Adv.* 2017;3: e1700156, 2017.

914 Butzin, M., Prange, M., Lohmann, G.: Radiocarbon simulations for the glacial ocean:
915 The effects of wind stress, Southern Ocean sea ice and Heinrich events. *Earth Planet.*
916 *Sci. Lett.*, 235, 45-61, 2005.

917 Butzin, M., Prange, M., and Lohmann, G.: Readjustment of glacial radiocarbon
918 chronologies by self-consistent three-dimensional ocean circulation modeling. *Earth*
919 *Planet Sci. Lett.*, 317, 177-184, 2012.

920 Butzin, M., Köhler, P., and Lohmann, G.: Marine radiocarbon reservoir age
921 simulations for the past 50,000 years. *Geophys. Res. Lett.*, 44, 8473–8480,
922 doi:10.1002/2017GL074688, 2017.

923 Butzin, M., Heaton, T.J., Köhler, P., and Lohmann, G.: A short note on marine
924 reservoir age simulations used in INTCAL20. *Radiocarbon*, oo, 1-7, DOI:10.1017/RDC.2020.9,
925 2020.

926 Chen, T., Robinson, L.F., Burke, A., Southon, J., Spooner, P., Morris, P.J., and Ng,
927 H.C.: Synchronous centennial abrupt events in the ocean and atmosphere during the
928 last deglaciation, *Science*, 349, 1537-1541, 2015.

929 Cheng, H., Edwards, R.L., Southon, J., Matsumoto, K., Feinberg, J.M., Sinha, A.,
930 Zhou, W., Li, H., Li, X., Xu, Y., Chen, S., Tan, M., Wang, Q., Wang, Y., and Ning, Y.:
931 Atmospheric $^{14}\text{C}/^{12}\text{C}$ changes during the last glacial period from Hulu Cave, *Science*,
932 362, 1293-1297, 2018.

933 Chikamoto, M.O., Abé-Ouchi, A., Oka, A., Ohgaito, R., and Timmermann, A.:
934 Quantifying the ocean's role in glacial CO_2 reductions, *Climate of the Past*, 8, 545–563,
935 doi:10.5194/cp-8-545-2012, 2012.

936 Cook M.S. and Keigwin L.D.: Radiocarbon profiles of the NW Pacific from the LGM
937 and deglaciation: Evaluating ventilation metrics and the effect of uncertain surface
938 reservoir ages, *Paleoceanography*, 30, 174–195, 2015.

939 Davies, S.M., Davies, P.M., Abbott, Meara, R.H., et al.: A North Atlantic tephro-
940 stratigraphical framework for 130-60 ka b2k: New tephra discoveries, marine based
941 correlations, and future challenges, *Quaternary Science Rev.*, 106, 101-121, 2014.

942 Du, J., Haley, B.A., Mix, A.C., Walczak, M.H., and Praetorius, S.K.: Flushing of the
943 deep Pacific Ocean and the deglacial rise of atmospheric CO_2 concentrations, *Nature*
944 *geoscience*, 11, 749-755, 2018.

945 Ferrari, R., Jansen, M.F., Adkins, J.F., Burke, A., Stewart, A.L., and Thompson, A.F.:
946 Antarctic sea ice control on ocean circulation in present and glacial climates, *Proc.*
947 *National Academy Science*, 111 (24), 8753–8758, 2014.

948 Gebbie, G.: How much did Glacial North Atlantic Water shoal? *Paleoceanography*,
949 29, 190-209, doi:10.1002/2013PA002557, 2014.

950 Gebhardt, H., Sarnthein, M., Kiefer, T., Erlenkeuser, H., Schmieder, F., and Röhl, U.:
951 Paleonutrient and productivity records from the subarctic North Pacific for Pleistocene
952 glacial terminations I to V. *Paleoceanography* 23, PA4212, 1-21,
953 doi:10.1029/2007PA001513, 2008.

954 Gong, S., Lembke-Jene, L., Lohmann, G., Knorr, G., Tiedemann, R., Zou, J.J and
955 Shi, X.F.: Enhanced North Pacific deep-ocean stratification by stronger intermediate
956 water formation during Heinrich Stadial 1. *Nature Communications*, 10: 656.

957 <https://doi.org/10.1038/s41467-019-08606-2>, 2019.

958 Grootes P.M. and Stuiver, M.: Oxygen 18/16 variability in Greenland snow and ice
959 with 1000 to 100000 year time resolution, *J. Geophys. Res.: Oceans* (1978–2012)
960 102(C12), 26455–26470, 1997.

961 Grootes, P.M. and Sarnthein, M.: Marine ¹⁴C reservoir ages oscillate, *PAGES News*,
962 14/3, 18-19, 2006.

963 Hain, M.P., Sigman, D.M., and Haug, G.H.: Distinct roles of the Southern Ocean and
964 North Atlantic in the deglacial atmospheric radiocarbon decline, *Earth Planetary Science*
965 *Letters* 394, 198-208, 2014.

966 Howe, J.N.W., Piotrowski, A.M., Noble, T.L., Mulitza, S., Chiessi, C.M., and Bayon,
967 G.: North Atlantic deep-water production during the last glacial maximum, *Nat.*
968 *Commun.*, 7, 11765, 2016. s

969 Howe, J.N.W., Huang, K-F., Oppo, D.W., Chiessi, C.M., Mulitza, S., Blusztajn, J.,
970 and Piotrowski, A.M.: Similar mid-depth Atlantic water mass provenance during the Last
971 Glacial Maximum and Heinrich Stadial 1, *Earth Planetary Science Letters*, 490, 51-61,
972 2018.

973 Jonkers, L. and Kucera, M.: Quantifying the effect of seasonal and vertical habitat
974 tracking on planktonic foraminifera proxies, *Climate of the Past*, 13, 573-586, 2017.

975 Keigwin, L.D. and Swift, S.A.: Carbon isotope evidence for a northern source of
976 deep water in the glacial western North Atlantic, *PNAS*, 114 (11), 2831-2835, 2017.

977 Key R. M., Kozyr, A., Sabine, C.L., Lee, K., Wanninkhof, R., Bullister, J.L., Feely,
978 R.A., Millero, F.J., Mordy, C., and Peng, T.-H. (2004) A global ocean carbon climat-
979 ology: Results from Global Data Analysis Project (GLODAP), *Global Biogeochem. Cy.*,
980 18, GB4031, doi:10.1029/2004GB002247, 2004.

981 Kong, X., Wang, Y., Wu, J., Cheng, H., Edwards, R.L., and Wang, X.: Complicated
982 responses of stalagmite $\delta^{13}\text{C}$ to climate change during the last glaciation from Hulu
983 Cave, Nanjing, China, *Science in China Ser. D Earth Sciences*, 48, (12), 2174-2181,
984 2005.

985 Küssner, K., Sarnthein, M., Lamy, F., and Tiedemann, R.: High-resolution
986 radiocarbon-based age records trace episodes of *Zoophycos* burrowing, *Marine*
987 *Geology*, 403, 48-56, <http://doi:10.1016/j.margeo.2018.04.01>, 2018.

988 Küssner, K., Sarnthein, M., Michel, E., Mollenhauer, G., Siani G., and Tiedemann,
989 R.: Glacial-to-deglacial reservoir ages of surface waters in the southern South Pacific.
990 *Paleoceanography and Paleoclimate*, 47 ms-pp. (under review).

991 Lascu, I., Feinberg, J.M., Dorale, J.A., Cheng, H., and Edwards, R.L.: Age of the
992 Laschamp excursion determined by U-Th dating of a speleothem geomagnetic record
993 from North America. *Geology*, 44, 139-142, doi:10.1130/G37490.1. 2016

994 Lindsay, C.M., Lehman, S.J., Marchitto, T.M., and Ortiz, J.D.: The surface
995 expression of radiocarbon anomalies near Baja California during deglaciation. *Earth
996 Planetary Science Letters*, 422, 67-74, 2015.

997 Lippold, J., Gutjahr, M., Blaser, P., Christner, E., de Cavalho-Fereira, M.L., Mulitza,
998 S. et al.: Deep-water provenance and dynamics of the (de)glacial Atlantic meridional
999 overturning circulation, *Earth Planetary Science Letters*, 445, 68-78, 2016.

1000 Lisiecki, L.E. and Stern, J.V.: Regional and global benthic $d^{18}O$ stacks for the last
1001 glacial cycle. *Paleoceanography*, 31, doi:10.1002/2016PA003002, 2016.

1002 Löwemark, L. and Grootes, P.M.: Large age differences between planktic
1003 foraminifers caused by abundance variations and Zoophycos bioturbation,
1004 *Paleoceanography*, 19, PA2001, doi:10.1029/2003PA000949, 2004.

1005 Marcott, S.A., Bauska, T.K., Buizert, C., Steig, E.J., Rosen, J.L., Cuffey, K.M.,
1006 Fudge, T.J., Severinghaus, J.P., Ahn, J., Kalk, M.L., McConnell, J.R., Sowers, T.,
1007 Taylor, K.C., White, J.W.C., and Brook, E.J.: Centennial-scale changes in the global
1008 carbon cycle during the last deglaciation, *Nature*, 514, 616-619,
1009 doi:10.1038/nature13799, 2014.

1010 Marshall, M., Schlolaut, G., Brauer, A., Nakagawa, T., Staff, R.A., Bronk Ramsey,
1011 C., Lamb, H., Gotanda, K., Haraguchi, T., Yokoyama, Y., Yonenobu, H., Tada, R.,
1012 SG06 project members: A novel approach to varve counting using μ XRF and X-
1013 radiography in combination with thin-section microscopy, applied to the Late Glacial
1014 chronology from Lake Suigetsu, Japan, *Quaternary Geochronology* 13, 70-80, 2012.

1015 McCave, I.N., Carter, I., and Hall, I.R.: Glacial-interglacial changes in water mass
1016 structure and flow in the SW Pacific Ocean, *Quaternary Science Rev.*, 27, 1886–1908,
1017 2008.

1018 Matsumoto, K.: Radiocarbon-based circulation age of the world oceans, *J. Geophys.
1019 Res.: Oceans* 112(C9), C09004. <https://doi.org/10.1029/2007JC004095>, 2007.

1020 Menviel, L., Spence, P., Yu, J., Chamberlain, M.A., Matear, R.J., Meissner K.J., and
1021 England, M.H.: Southern Hemisphere westerlies as a driver of the early deglacial
1022 atmospheric CO₂ rise, *Nature communications*, 9:2503, DOI:10.1038/s41467-018-
1023 04876-4, 2018.

1024 Millo, C., Sarnthein, M., and Erlenkeuser, M.: Variability of the Denmark Strait
1025 Overflow during the Last Glacial Maximum, *Boreas*, 35, 50-60, 2006.

1026 Muglia, J., Skinner, L., and Schmittner, A.: Weak overturning circulation and high
1027 Southern Ocean nutrient utilization maximized glacial ocean carbon, *Earth and*
1028 *Planetary Science Letters* 496, 47-56, 2018.

1029 Muschitiello, F., D'Andrea, W.J., Schmittner, A., Heaton, T.J., Balascio, N.L.,
1030 deRoberts, N., Caffee, M.W., Woodruff, T.E., Welten, K.C., Skinner, L.C., Simon, M.H.,
1031 and Dokken T.M.: Deep-water circulation changes lead North Atlantic climate during
1032 deglaciation, *Nature Communications* 10, 1272, doi.org/10.1038/s41467-019-09237-3,
1033 2019.

1034 Naughton, F., Costas, S., Gomes, S.D., Desprat, S., Rodrigues, T., Sanchez Goñi,
1035 M.F., Renssen, H., Trigo, R., Bronk-Ramsey, C., Oliveira, D., Salgueiro, E., Voelker,
1036 A.H.L., and Abrantes, F.: Coupled ocean and atmospheric changes during Greenland
1037 stadial 1 in southwestern Europe, *Quaternary Science Reviews*, 212, 108-120, 2019.

1038 Nydal R., Lovseth K., and Skogseth F. H.: Transfer of bomb ^{14}C to the ocean
1039 surface, *Radiocarbon* 22(3), 626–635, 1980.

1040 Okazaki, Y., Sagawa, T., Asahi, H., Horikawa, K., and Onodera, J.: Ventilation
1041 changes in the western North Pacific since the last glacial period, *Climate of the Past*, 8,
1042 17-24, doi:10.5194/cp-8-17-2012, 2012.

1043 Paillard, D., Labeyrie, L., and Yiou, P.: Macintosh program performs time-series
1044 analysis, *Eos Trans, AGU*, 77: 379, 1996.

1045 Rae, J.W.B. and W. Broecker, W.: What fraction of the Pacific and Indian oceans'
1046 deep water is formed in the Southern Ocean? *Biogeosciences*, 15, 3779-3794, 2018.

1047 Rae, J., Sarnthein, M., Foster, G., Ridgwell, A., Grootes, P.M., and Elliott T.: Deep
1048 water formation in the North Pacific and deglacial CO_2 rise, *Paleoceanography*, 29,
1049 doi:10.1002/2013PA002570, 645–667, 2014.

1050 Rafter, P.A., Herguera, J.-C., and Southon, J.R.: Extreme lowering of deglacial
1051 seawater radiocarbon recorded by both epifaunal and infaunal benthic foraminifera in a
1052 wood-dated sediment core, *Climate of the Past* 14, 1977–1989, 2018.

1053 Reimer P.J., Bard, E., Bayliss, A., Beck, J. W., Blackwell, P.G., Bronk Ramsey, C.,
1054 Buck, C.E., Cheng, H., Edwards, R.L., and Friedrich, M.: IntCal13 and Marine13
1055 radiocarbon age calibration curves 0–50,000 years cal. BP, *Radiocarbon* 55, 1869–
1056 1887, 2013.

1057 Reimer, P.J., et al.: The IntCal 20 northern hemisphere radiocarbon calibration curve
1058 (0-55 kcal BP), *Radiocarbon*, 2020 (in press).

1059 Robinson, L.F., Adkins, J.F., Keigwin, L.D., et al.: Radiocarbon variability in the
1060 western North Atlantic during the last deglaciation, *Science*, 310, 1469-1473, 2005.

1061 Ronge, T. A., Tiedemann, R., Lamy, F., et al.: Radiocarbon constraints on the extent
1062 and evolution of the South Pacific glacial carbon pool, *Nature Comm.* 7:11487, 2016.

1063 Ronge, T.A., Sarnthein, M., Roberts, J., Lamy, F., and Tiedemann, R.: East Pacific
1064 Core PS75/059-2: Glacial-to-deglacial stratigraphy revisited, *Paleoceanography and*
1065 *Paleoclimatology*, 34 (4), 432-435, DOI:10.1029/2019PA003569, 2019.

1066 Sarnthein, M., Winn, K., Jung, S.J., Duplessy, J.C., Labeyrie, L., Erlenkeuser, H.,
1067 and Ganssen, G.: Changes in east Atlantic deepwater circulation over the last 30,000
1068 years: eight time slice reconstructions, *Paleoceanography*, 9(2), 209–267, 1994.

1069 Sarnthein, M., Pflaumann, U., and Weinelt, M.: Past extent of sea ice in the northern
1070 North Atlantic inferred from foraminiferal paleotemperature estimates,
1071 *Paleoceanography*, 18(2), 2003.

1072 Sarnthein, M., Grootes, P.M., Kennett, J.P., and Nadeau, M.: ¹⁴C Reservoir ages
1073 show deglacial changes in ocean currents and carbon cycle, *Geophys. Monograph –*
1074 *Am. Geophys. Union*, 173, 175–196, 2007.

1075 Sarnthein, M., Grootes, P.M., Holbourn, A., Kuhnt, W., and Kühn, H.: Tropical
1076 warming in the Timor Sea led deglacial Antarctic warming and almost coeval
1077 atmospheric CO₂ rise by >500 yr, *Earth Planetary Science Letters*, 302, 337-348, 2011.

1078 Sarnthein, M., Schneider, B., and Grootes, P.M.: Peak glacial ¹⁴C ventilation ages
1079 suggest major draw-down of carbon into the abyssal ocean, *Climate of the Past*, 9 (1),
1080 925–965, 2013.

1081 Sarnthein, M., Balmer, S., Grootes, P.M., and Mudelsee, M.: Planktic and benthic
1082 ¹⁴C reservoir ages for three ocean basins, calibrated by a suite of ¹⁴C plateaus in the
1083 glacial-to-deglacial Suigetsu atmospheric ¹⁴C record, *Radiocarbon*, 57, 129–151, 2015.

1084 Sarnthein, M. and Werner, K.: Early Holocene planktic foraminifers record species-
1085 specific ¹⁴C reservoir ages in Arctic Gateway, *Marine Micropaleontology*, 135, 45-55.
1086 DOI:10.1016/j.marmicro.2017.07.002, 2018.

1087 Schlolaut, G.: A unique and easy-to-use-tool to deal with incompletely varved
1088 archives 782 – the Varve Interpolation Program 3.0.0, *Quaternary Geochronology*, 2019
1089 (in press).

1090 Schlolaut, G., Staff, R.A., Marshall, M.H., Brauer, A., Bronk Ramsey, C., Lamb, H.F.,
1091 and Nakagawa, T.: Microfacies analysis of the Lake Suigetsu (Japan) sediments from
1092 ~50 to ~10 ka BP and an extended and revised varve based chronology, *Quaternary*
1093 *Science Reviews*, 200, 351-366, 2018.

1094 Schmittner, A. and Lund, D.C.: Early deglacial Atlantic overturning decline and its
1095 role in atmospheric CO₂ rise inferred from carbon isotopes ($\delta^{13}\text{C}$), *Climate of the Past*,
1096 11, 135-152, 2015.

1097 Schroeder, J., Holbourn, A., Küssner, K., and Kuhnt, W.: Hydrological variability in
1098 the southern Makassar Strait during the last glacial termination, *Quaternary Science*
1099 *Reviews*, 154, 143-156, 2016.

1100 Sessford, E.G., Jensen, M.F., Tisserand, A.A., Muschitiello, F., Dokken, T.,
1101 Nisancioglu, K.H., and Jansen, E.: Consistent fluctuations on intermediate water
1102 temperature off the coast off Greenland and Norway during Dansgaard-Oeschger
1103 events, *Quaternary Science Reviews*, 223, 105887, 1-17, 2019.

1104 Sherriff-Tadano, S., Abe-Ouchi, A., Yoshimori, M., Oka, A., and Chan, W.-L.:
1105 (Influence of glacial ice sheets on the Atlantic meridional overturning circulation through
1106 surface wind change, *Climate Dynamics*, 50 (7-8), 2881–2903, 2017.

1107 Siani, G., Michel, E., De Pol-Holz, R., DeVries, T., Lamy, F., Carel, M., Isguder, G.,
1108 Dewilde, F., Laurantou, A.: Carbon isotope records reveal precise timing of enhanced
1109 Southern Ocean upwelling during the last deglaciation, *Nature Communications*, 4,
1110 2758, 2013.

1111 Sikes, E.L. and Guilderson, T.P.: Southwest Pacific Ocean surface reservoir ages
1112 since the last deglaciation: Circulation insights from multiple-core studies. *Paleocean-*
1113 *ography*, 31, 298–310, doi:10.1002/2015PA002855, 2016.

1114 Simstich, J., Sarnthein, M., and Erlenkeuser, H.: Paired $\delta^{18}\text{O}$ signals of
1115 *Neogloboquadrina pachyderma* (s) and *Turborotalita quinqueloba* show thermal
1116 stratification structure in Nordic Seas, *Mar. Micropaleontol.*, 912, 1–19, 2003.

1117 Skinner, L.C., Fallon, S., Waelbroeck, C., Michel, E., and Barker, S.: Ventilation of
1118 the deep Southern Ocean and deglacial CO₂ rise, *Science*, 328, 1147–1151, 2010.

1119 Skinner, L.C., Waelbroeck, C., Scrivner, A.E., and Fallon, S.J.: Radiocarbon
1120 evidence for alternating northern and southern sources of ventilation of the deep
1121 Atlantic carbon pool during the last deglaciation, *PNAS*, 111, 5480–5484, 2014.

1122 Skinner, L.C. *et al.*: Reduced ventilation and enhanced magnitude of the deep
1123 Pacific carbon pool during the last glacial period, *Earth Planetary Science Letters*, **411**,
1124 45-52, 2015.

1125 Skinner, L.C., Primeau, F., Freeman, E., de la Fuente, M., Goodwin, P.A.,
1126 Gottschalk, J., Huang, E., McCave, I.N., Noble, T.L., and Scrivner A.E.: Radiocarbon
1127 constraints on the glacial ocean circulation and its impact on atmospheric CO₂, *Nature*
1128 *communications*, 8:16010, DOI: 10.1038/ncomms16010, 2017.

1129 Skinner, L.C., Muschitiello, F., and Scrivner, A.E.: Marine reservoir age variability
1130 over the last deglaciation: Implications for marine carbon cycling and prospects for
1131 regional radiocarbon calibrations. *Paleoceanography and Paleoclimate*, 34,
1132 doi.org/10.1029/2019PA003667, 2019.

1133 Southon, J., Noronha, A.L., Cheng, H, Edwards, R.L., and Wang, Y.: A high-
1134 resolution record of atmospheric ¹⁴C based on Hulu Cave speleothem H82, *Quaternary*
1135 *Science Reviews*, 33:32-41, 2012.

1136 Steffensen, J.P., Andersen, K.K., Bigler, M., et al.: High-Resolution Greenland Ice
1137 Core Data Show Abrupt Climate Change Happens in Few Years, *Science*, 321, 680;
1138 DOI: 10.1126/science.1157707, 2008.

1139 Stern, J.V. and Lisiecki, L.E.: North Atlantic circulation and reservoir age changes
1140 over the past 41,000 years, *Geophysical Research Letters*, 40, 3693-3697,
1141 doi:10.1002/grl.5067, 2013.

1142 Stocker, T. and Johnsen, S.J.: A minimum thermodynamic model for the bipolar
1143 seesaw, *Paleoceanography*, 18 (4), 1087, doi:10.1029/2003PA000920, 2003.

1144 Stuiver, M. and Braziunas, T.V.: Modeling atmospheric ¹⁴C influences and ¹⁴C ages
1145 of marine samples to 10,000 B.C., *Radiocarbon*, 35, 137–189, 1993.

1146 Svensson, A., Andersen, K.K., Bigler, M., Clausen, H.B., Dahl-Jensen, D., Davies,
1147 S.M., Johnsen, S.J., Muscheler, R., Parrenin, F., Rasmussen, S.O., Röthlisberger, R.,
1148 Seierstad, I., Steffensen, J.P., and Vinther, B.M.: A 60 000 year Greenland stratigraphic
1149 ice core chronology, *Climate of the Past*, 4, 47–57, 2008.

1150 Toggweiler, J.R., Druffel, E.R.M., Key, R.M., and Galbraith, E.D.: Upwelling in the
1151 ocean basins north of the ACC. Part 2: How cool Subantarctic water reaches the
1152 surface in the tropics, *J. Geophysical Research*, DOI:[10.1029/2018JC014795](https://doi.org/10.1029/2018JC014795), 2019 (in
1153 press).

1154 Turney, C.S.M., Fifield, L.K., Hogg, A.G., et al.: Using New Zealand kauri (*Agathis*
1155 *australis*) to test the synchronicity of abrupt climate change during the Last Glacial

1156 Interval (60,000–11,700 years ago), *Quatern. Sci. Rev.*, 29, 3677–3682, 2010.

1157 Turney, C.S.M., Jones, R.T., Phipps, S.J., et al.: Rapid global ocean-atmosphere
1158 response to Southern Ocean freshening during the last glacial, *Nature communications*,
1159 8:520, doi:10.1038/s41467-017-00577-6, 2017.

1160 Umling, N.E. and Thunell, R.C.: Synchronous deglacial thermocline and deep-
1161 water ventilation in the eastern equatorial Pacific, *Nature communications*, 8, 14203.
1162 DOI: 10.1038/ncomms14203, 2017.

1163 Waelbroeck, C., Duplessy, J.-C., Michel, E., Labeyrie, L., Paillard, D., and Duprat, J.:
1164 The timing of the last deglaciation in North Atlantic climate records, *Nature*, 412, 724–
1165 727, 2001.

1166 Waelbroeck, C., Skinner, L.C., Labeyrie, L., Duplessy, J.-C., Michel, E., Riveiros,
1167 N.V., Gherardi, J.-M., and Dewilde, F.: The timing of deglacial circulation changes in the
1168 Atlantic, *Paleoceanography*, 26, PA3213, <https://doi.org/10.1029/2010PA002007>, 2011.

1169 Wallmann, K., Schneider, B., and Sarnthein, M.: Effects of eustatic sea-level
1170 change, ocean dynamics, and nutrient utilization on atmospheric pCO₂ and seawater
1171 composition over the last 130,000 years – a model study, *Climate of the Past*, 12, 339-
1172 375, doi: 10.5194/cp-12-339-2016, 2016.

1173 Wang Y.C, Cheng, H., Edwards, R.L., An, Z.S., Wu, J.Y., Shen, C.-C., and Dorale,
1174 J.A.: A high-resolution absolute-dated Late Pleistocene monsoon record from Hulu
1175 Cave, China, *Science*, 294, 2345-2348. DOI: 10.1126/science.1064618, 2001.

1176 Wang, L.J., Sarnthein, M., Erlenkeuser, H., Grimalt, J., Grootes, P., Heilig, S.,
1177 Ivanova, E., Kienast, M., Pelejero, C., and Pflaumann, U.: East Asian monsoon climate
1178 during the late Pleistocene: High-resolution sediment records from the South China
1179 Sea, *Marine Geology*, 156, 245-284, 1999.

1180 Wang, P., Clemens, S., Beaufort, L., Braconnot, P., Ganssen, G., Jian, Z., Kershaw,
1181 P., and Sarnthein, M.: SCOR/IMAGES Working Group 113 SEAMONS: Evolution and
1182 variability of the Asian Monsoon System: State of the art and outstanding issues,
1183 *Quaternary Science Reviews*, 24 (5-6), 595-629, 2005.

1184 WAIS Divide Project Members: Onset of deglacial warming in West Antarctica driven
1185 by local orbital forcing. *Nature*, 500, 440-444. doi:10.1038/nature12376, 2013.

1186 Xu, J., Kuhnt, W., Holbourn, A., Regenber, M., and Andersen, N.: Indo-Pacific
1187 Warm Pool variability during the Holocene and Last Glacial Maximum, *Paleoceanogr.*,
1188 25, 16, 2010.

1189 Yamamoto, A., Abe-Ouchi, A., Ohgaito, R., Ito, A., and Oka, A.: Glacial CO₂

1190 decrease and deep-water deoxygenation by iron fertilization from glaciogenic dust,
1191 *Climate of the Past*, 15, 981-996.

1192 Yashayaev, I., Seidov, D., and Demirov, E.: A new collective view of oceanography
1193 of the Arctic and North Atlantic basins, *Progress in Oceanography*, 132, 21 pp.,
1194 DOI:<http://dx.doi.org/10.1016/j.pocean.2014.12.012>, 2015.

1195 Zhao, N. and Keigwin, L.D.: An atmospheric chronology for the glacial-deglacial
1196 Eastern Equatorial Pacific, *Nature communications*, 9:3077, DOI:10.1038/s41467-018-
1197 05574-x, 2018.

1198 Zhao, N., Marchal, O., Keigwin, L., Amrhein, D., and Gebbie, G.: A synthesis of
1199 deep-sea radiocarbon records and their (in) consistency with modern ocean ventilation,
1200 *Paleoceanography and Paleoclimatology*, 33, 128-151, 2018.

1201 TABLE CAPTIONS

1202

1203 **Table 1 a and b.** Summary of varve- and U/Th model-based age estimates (Schlolut
 1204 et al., 2018; Bronk Ramsey et al., 2012) for ~30 plateau (pl.) boundaries in the
 1205 atmospheric ¹⁴C record identified in Lake Suigetsu Core SG06₂₀₁₂ by means of visual
 1206 inspection over the interval 10.5–27 cal. ka (Sarnthein et al., 2015, suppl. and modified).
 1207 At the right hand side, three columns give the average (Ø) and uncertainty range of ¹⁴C
 1208 ages for each ¹⁴C plateau.

SUIGETSU Plateau Top		Depth	Plateau Base		Depth	Ø 14C Age	±Uncertainty	14C age BP	
SG06_2012	Varve-based	U/Th-based	(cm c.d.)	Varve-based	U/Th-based	(cm c.d.)	of 14C Plateau	(14C yr)	min/max.
Plateau no.	age (yr BP)	age (yr BP)		age (yr BP)	age (yr BP)		(14C yr)		(1.6 σ range)
'Preboreal'	10525	10560	1325	11100	11108	1383	9525	−170/+110	9356/ 9635
'Top YD'	11290	11281	1402	11760	11755	1453	10060	−100/+35	9963/ 10095
'YD'	11950	11895	1467	12490	12475	1525	10380	−170/ 124	10211/ 10504
'no name'	12885	12780	1555	13160	13080	1582	11000	−85/ 114	10915/ 11114
1a	13580	13656	1626	13980	14042	1657	12006	100	11857/ 12050
1	14095	14160	1666	15095	15100	1740	12471	185	12315/ 12683
2a	15310	15420	1754	16140	16520	1802	13406	245	13174/ 13665
2b	16075	16520	1802	16400	16930	1820	13850	40	13808/ 13885
3	16835	17500	1847	17500	18220	1888	14671	105	14582/ 14792
4	17880	18650	1913	18830	19590	1971	15851	190	15661/ 16044

1209

5a	18960	19720	1978	19305	20240	2003	16670	90	16570/ 16750
5b	19305	20240	2003	20000	20900	2032	17007	190	16830/ 17247
6a	20190	21000	2050	20920	21890	2105	17667	262	17435/ 17960
6b	20920	21890	2105	21275	22300	2132	18075	140	17960/ 18240
7	21375	22400	2140	21790	22870	2171	18843	117	18741/ 18975
8	21835	22940	2175	22730	24250	2257	19715	-290 325	19425/ 20041
9	22730	24250	2257	23395	25150	2312	20465	-227 263	20238/ 20728
10a	23935	25880	2358	25080	27000	2400	22328	-380 270	21946/ 22600
10b	25080	27000	2400	25800	27600	2426	22708	-475 440	22233/ 23147
11	26110	27770	2443	27265	28730	2525	24088	-360 505	23727/ 24595

1210

1211

1212 √ **Table 2.** Temporal match of various ¹⁴C plateaus with deglacial periods of major
 1213 atmospheric CO₂ rise and ocean warmings (AA = Antarctic; GIS = Greenland
 1214 Interstadial).

DEGLACIAL EVENTS of pCO₂ RISE vs. age of pla. ¹⁴C PLATEAUS (in cal. ka)

pCO ₂ RISE (~12 ppm)	Plateau no.	Plateau boundaries
AGE based on annual layers AA ice core (Marcott et al. 2014)		AGE range (cal. ka) based on U/Th model ages (Bronk Ramsey et al., 2012)
11.7 – 11.5	# 'Top YD'	11.83 – 11.3
14.8 – 14.53	# 1	15.1 – 14.2
16.4 – 16.15	# 2a	16.52 – 15.5
17.4 – ~17.1	(data gap)	17.3 – 17.1

FURTHER POTENTIAL CORRELATIVES:

Progressive N. Atlantic warming during the YD at 12.39 – 12.03 ka *	# 'YD'	12.46 – 11.98
Onset of Antarctic ** warming at 18.3–17.6 ka (ice-based time scale)	#3	18.22 – 17.5
Onset of North Atlantic *** warming at 19.3–18.6 ka (U/Th-based time scale)	# 4	19.6 – 18.65
Top H2: GIS 2 N. Atlantic warming at 23.4 – 23.3 ka ****	#8	24.25 – 22.95

AGE CONTROL based on

* Naughton et al. (2019), ** Kawamura et al. (2007),

*** Balmer and Sarnthein (2018), **** Grootes and Stuiver (1997)

1215

1216 **Table 3** a-c. ¹⁴C reservoir / ventilation ages of surface (top 50-100 m) and bottom
 1217 waters vs. U/Th-based model age at 19/22 core sites in the ocean. (a) Spatial and
 1218 temporal changes over early and late LGM (24–21 and 21–18.7 cal. ka), (b) HS-1, and
 1219 the B/A. Late LGM estimates (average res. age of Plateau 4-5) are compared to model-
 1220 based estimates of Muglia et al. (2018). (c) Data sources. For core locations see Fig. 7.
 1221 (a)

Sediment Core U/Th-based model age Plateau (Pl.) no.	Latitude	Longitude	Water depth (m)	LGM pla. res. age		LGM model		res. age	
				24–21 ka (early LGM) Pl. 8 - 7 - 6 Error (yr)	21–18.7 ka (late LGM) Pl. 5 - 4 Error (yr)	strong AMOC	weak		
ATLANTIC O.									
PS2644	67°52.02'N	21°45.92'W	777	2100	±390	1920–2200	±325–±120	1136	1100
GIK 23074	66°66.67'N	4°90'E	1157	620–790	±145–±270	550–1175	±100–±200	1054	1059
MD08-3180	38°N	31°13.45'W	3064	–	–	320–605	±125–±405	827	887
SHAK06-5K (= MD99-2334)	37°34'N (37°48'N)	10°09'W 10°10'W	2646 3146	675–800	–	500–660	–	872	855
ODP 1002	10°42.37'N	65°10.18'W	893	700–210	±230–±310	25 – -205	±205–±215	751	738
GeoB 3910-1	4°15'S	36°21'W	2361	–	–	–	–	779	796
GeoB 1711-4	23°17'S	12°23'W	1976	1080	±290	730–840	±240–±190	711	721
KNR 159-5-36GGC	27°31'S	46°48'W	1268	540	±140	870	±120	757	777
MD07-3076	44°4'S	4°12'W	3770	–	–	2300	±200	928	989
INDIAN O./TIMOR SEA									
MD01-2378	13°08.25'S	121°78.8'E	1783	–	–	2000–1700	±300–±320	885	890
PACIFIC O.									
MD02-2489	54°39.07'N	148°92.13'W	3640	–	–	1560–1110	±310–±335	972	965
MD01-2416	51°26.8'N	167°72.5'E	2317	–	–	1710	±440	1227	1202
ODP 893A	34°17.25'N	120°02.33'W	588	–	–	1065	±280	839	846
MD02-2503	34°16.6'N	120°01.6'W	580	–	–	–	–	839	846
GIK 17940	20°07.0'N	117°23.0'E	1727	1820–1260	±320–±230	hiatus	–	836	838
(= SO50-37)	18°55'N	115°55'E	2655	1820–1260	–	–	–	836	840
PS75/104-1	44°46'S	174°31'E	835	1650–1280	±210–±320	1500	±340	881	895
(= SO213-84)	45°7.5'S	174°34.9'E	972	1650–1280	±210–±320	1500	±340	881	895
MD07-3088	46°S	75°W	1536	385	±315	380-450	±140–±230	917	–
SO213-76-2	46°13'S	178°1.7'W	4339	–	–	1460–990	±340–±550	915	842
PS97/137-1	52°39.5'S	75°33.9'E	1027	600–1180	±465	1180–800	±90–±225	1505	1419

1222

1223 (b)

Sediment Core U/Th-based model at Plateau (Pl.) no.	HS-1 pla. res. age		16.5–15.5 ka		B/A pla. res. age		LGM be. vent age		LGM b.w. model age	
	18–16.5 ka	16.5–15.5 ka	14.7–13.6 ka	(yr)	early	late	strong	AMOC	weak	(yr)
ATLANTIC O.										
PS2644	1775–1660	±105–±160	1900	±355	–	345	2400	948	918	
GIK 23074	1730–2000	±125–±160	670	±310	140–310	±250–±100	375	375	960	931
MD08-3180	1420–1610	±310–±160	1460	±390	630–360	±310	600	600	1031	1004
SHAK06-5K (= MD99-2334)	330–410		535		780–925		—	—	—	—
ODP 1002	–100 – 20	±140	90	±345	355	±200	—	2200–2700	1900	—
GeoB 3910-1	630–560	±160–±180	175	±475	210–230	±220–±110	2150	2150	—	—
GeoB 1711-4	660–690	±195–±45	420	±320	880	±255	1500	1500	1387	1714
KNR 159-5-36GGC	460–340	±380–±300	170	±700	180–230	±370–±310	1470	1470	1354	1563
MD07-3076	1650	±180	–		920	±230	3640	3640	1653	2060
INDIAN O./TIMOR SEA										
MD01-2378	740	±125	–		200–185	±345–±130	2720	—	1679	1881
PACIFIC O.										
MD02-2489	800–550	±155–±120	550	±305	440	±285	—	2625	2332	2595
MD01-2416	1480–1140	±135–±190	–		720–570	±285–±140	—	3700/5100	2400	2683
ODP 893A	1065–1490	±280–±120	1400	±370	520	±185	—	1430	1677	1705
MD02-2503	965–1365	±160–±160	1215	±325	395–535	±240–±130	—	—	—	—
GIK 17940 (= SO50-37)	1210–1370	±200–±470	1045	±320	870–970	±325–±100	3300–1800	—	1807	1897
PS75/104-1 (= SO213-84)	1050	±265	1180	±350	800	±280	—	3225	3225	2373
MD07-3088	800–1090	±85–±125	1060	±275	1310–730	±125–±190	1500	2400	1101	1146
SO213-76-2	840	±310	–		–	–	1360 ?	1600	1808	1701
PS97/137-1	1500–670	±90–±180	455	±270	–	–	1400–2400	2400/2900	1631	1871

1224

1225 (c)

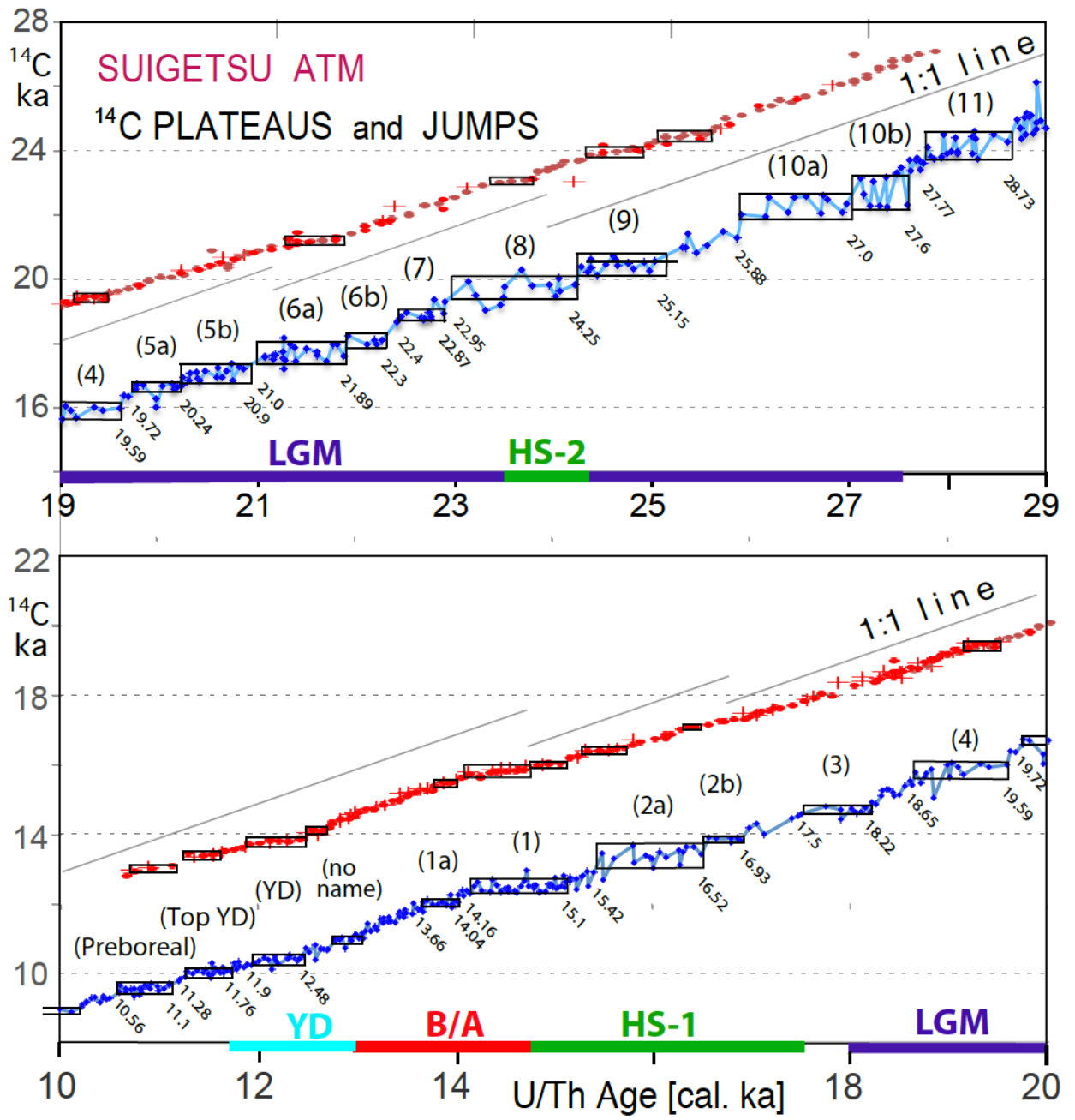
Sediment Core	DATA Source
ATLANTIC O.	
PS2644	Sarnthein et al. 2015
GIK 23074	Sarnthein et al. 2015
MD08-3180	Balmer et al. 2018
SHAK06-5K (= MD99-2334)	Ausin et al., 2020 subm.
ODP 1002	Skinner et al. 2014
GeoB 3910-1	Sarnthein et al. 2015
GeoB 1711-4	Balmer et al. 2016
KNR 159-5-36GGC	Balmer et al. 2016
MD07-3076	Balmer et al. 2016
INDIAN O./TIMOR SEA	
MD01-2378	Sarnthein et al. 2015
PACIFIC O.	
MD02-2489	Sarnthein et al. 2015
MD01-2416	Sarnthein et al. 2015
ODP 893A	Sarnthein et al. 2015
MD02-2503	Sarnthein et al. 2015
GIK 17940 (= SO50-37)	Sarnthein et al. 2015
PS75/104-1 (= SO213-84)	Sarnthein et al. 2015
MD07-3088	Küssner et al., 2020 subm
SO213-76-2	Siani et al. 2013
PS97/137-1	Ronge et al. 2016
	Küssner et al., 2020 subm
	data suppl.

1226 (c)

1227 FIGURE CAPTIONS

1228

1229 – Fig. 1. Atmospheric ^{14}C ages of Lake Suigetsu plant macrofossils 10–20 cal. ka
1230 (bottom panel) and 19–29 cal. ka (top panel) vs. U/Th-based model age (blue dots;
1231 Bronk Ramsey et al., 2012). The 1:1 line reflects gradient of one ^{14}C yr / cal. yr. Double
1232 and triple ^{14}C measurements are averaged. (In part large) error bars of single ^{14}C ages
1233 are given in Suppl. Fig. S1. Suite of labeled horizontal boxes that envelop scatter bands
1234 of largely constant ^{14}C ages shows ^{14}C plateaus longer than 250 yr (plateau boundary
1235 ages listed in Table 1). Red and brown dots (powder samples from trench and wall) and
1236 + signs (off-axis samples) depict raw ^{14}C ages of Hulu stalagmites H82 and MSD
1237 (Cheng et al., 2018; Southon et al., 2012; plot offset by +3000 ^{14}C yr). Suite of short ^{14}C
1238 plateaus (black boxes) tentatively assigned to Hulu-based record occupies age ranges
1239 slightly different from those deduced for Suigetsu-based plateaus. The difference
1240 possibly results from short-term changes in the Old / Dead Carbon Fraction (ocf / dcf)
1241 that in turn may reflect major short-term changes in LGM and deglacial monsoon
1242 climate (Wang et al., 2001; Kong et al., 2005).

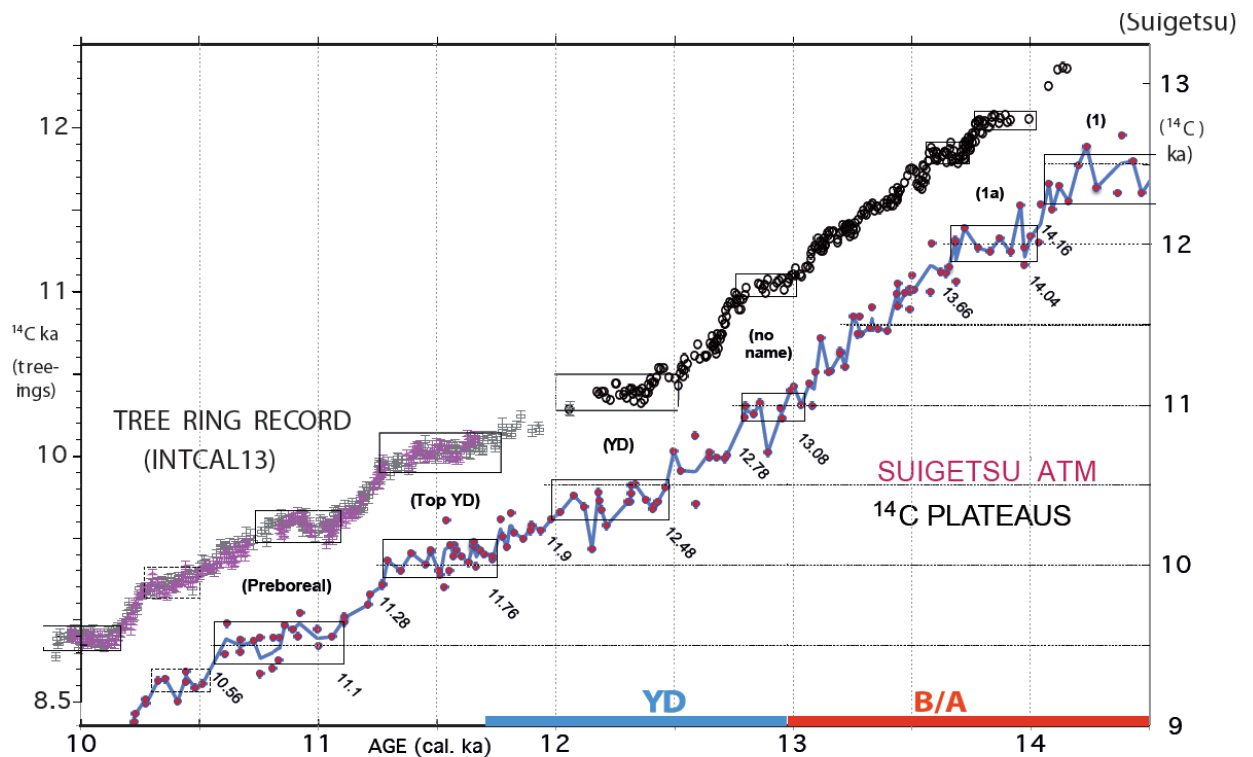


1243

1244

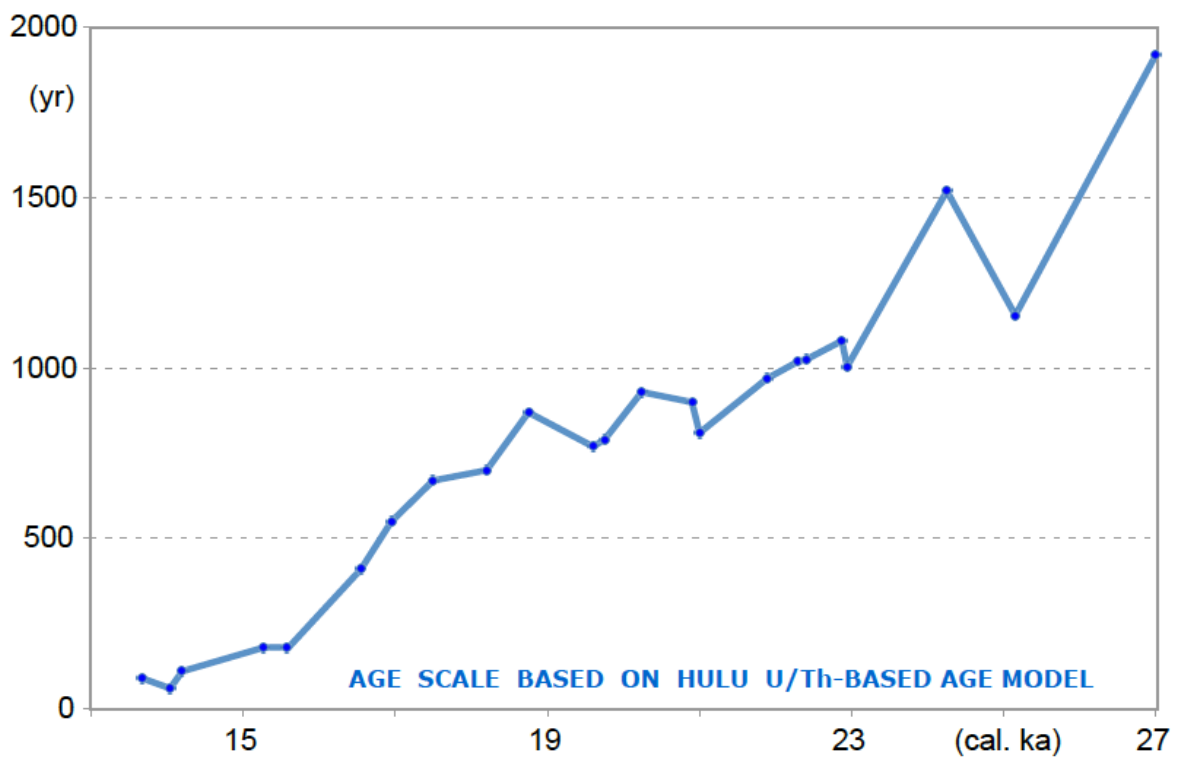
1245

1246 √ Fig. 2. High-resolution record of atmospheric ^{14}C jumps and plateaus (= suite of
 1247 labeled horizontal boxes that envelop scatter bands of largely constant ^{14}C ages
 1248 extending over >300 cal. yr) in a sediment section of Lake Suigetsu vs. tree ring-based
 1249 ^{14}C jumps and plateaus 10–14.5 cal. ka (Reimer et al., 2013). Blue line averages paired
 1250 double and triple ^{14}C ages of Suigetsu plant macrofossils. Age control points (cal. ka)
 1251 follow varve counts (Scholaut et al., 2018) and U/Th model-based ages of Bronk
 1252 Ramsey et al. (2012). YD = Younger Dryas, B/A = Bølling-Allerød.
 1253



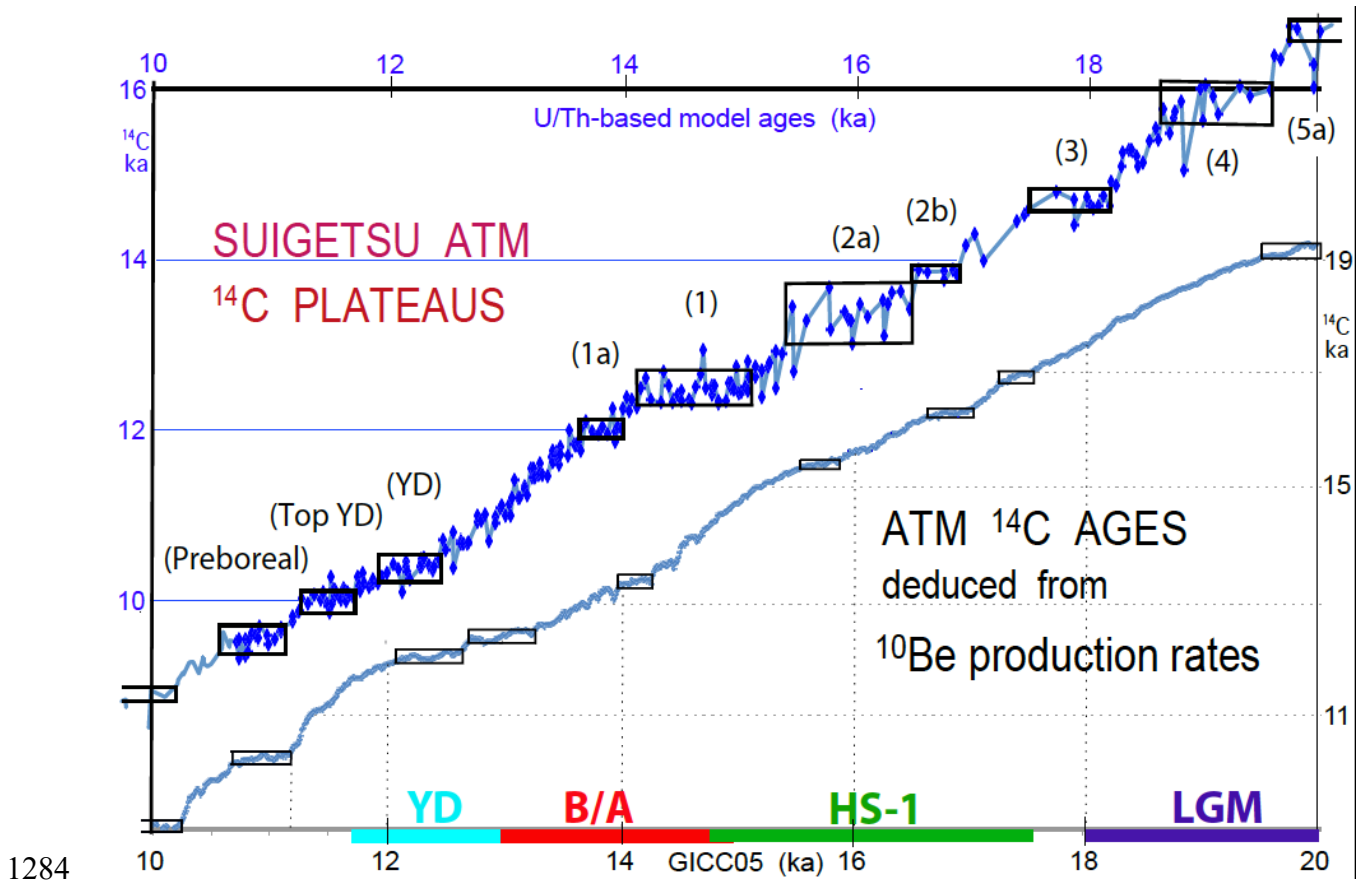
1254
 1255
 1256
 1257
 1258
 1259
 1260
 1261
 1262
 1263
 1264

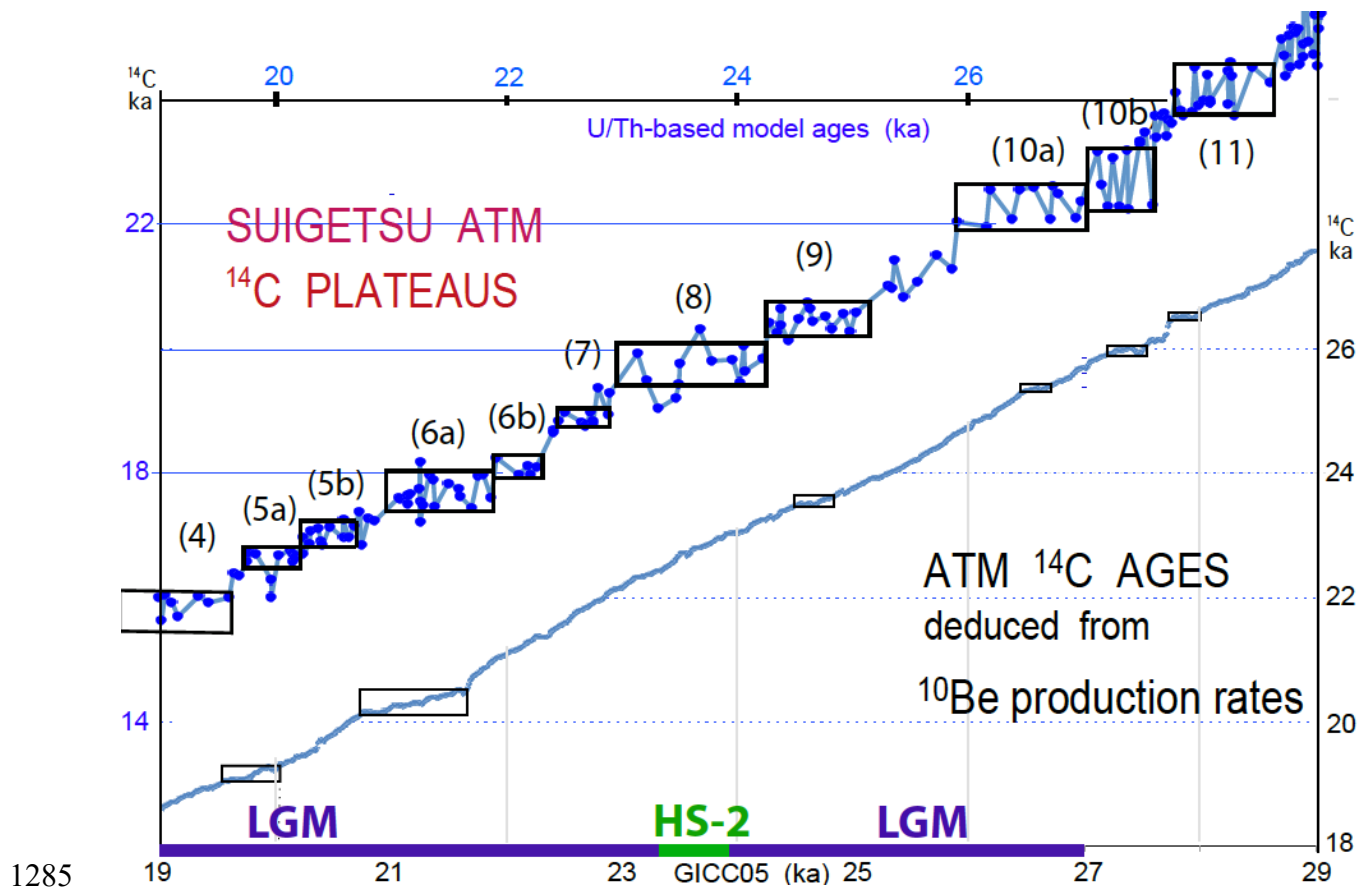
1265 √ Fig. 3. Difference between Hulu Cave U/Th-based model ages (Southon et al., 2012;
1266 Bronk Ramsey et al., 2012; Cheng et al., 2018) and varve count-based cal. ages for
1267 atmospheric ¹⁴C plateau boundaries in Lake Suigetsu sediment record (Schlollaut et al.,
1268 Sarnthein et al., 2015, suppl. and revised), displayed on the U/Th-based time
1269 scale 13–27 cal. ka.
1270



1271
1272
1273
1274
1275
1276
1277
1278
1279

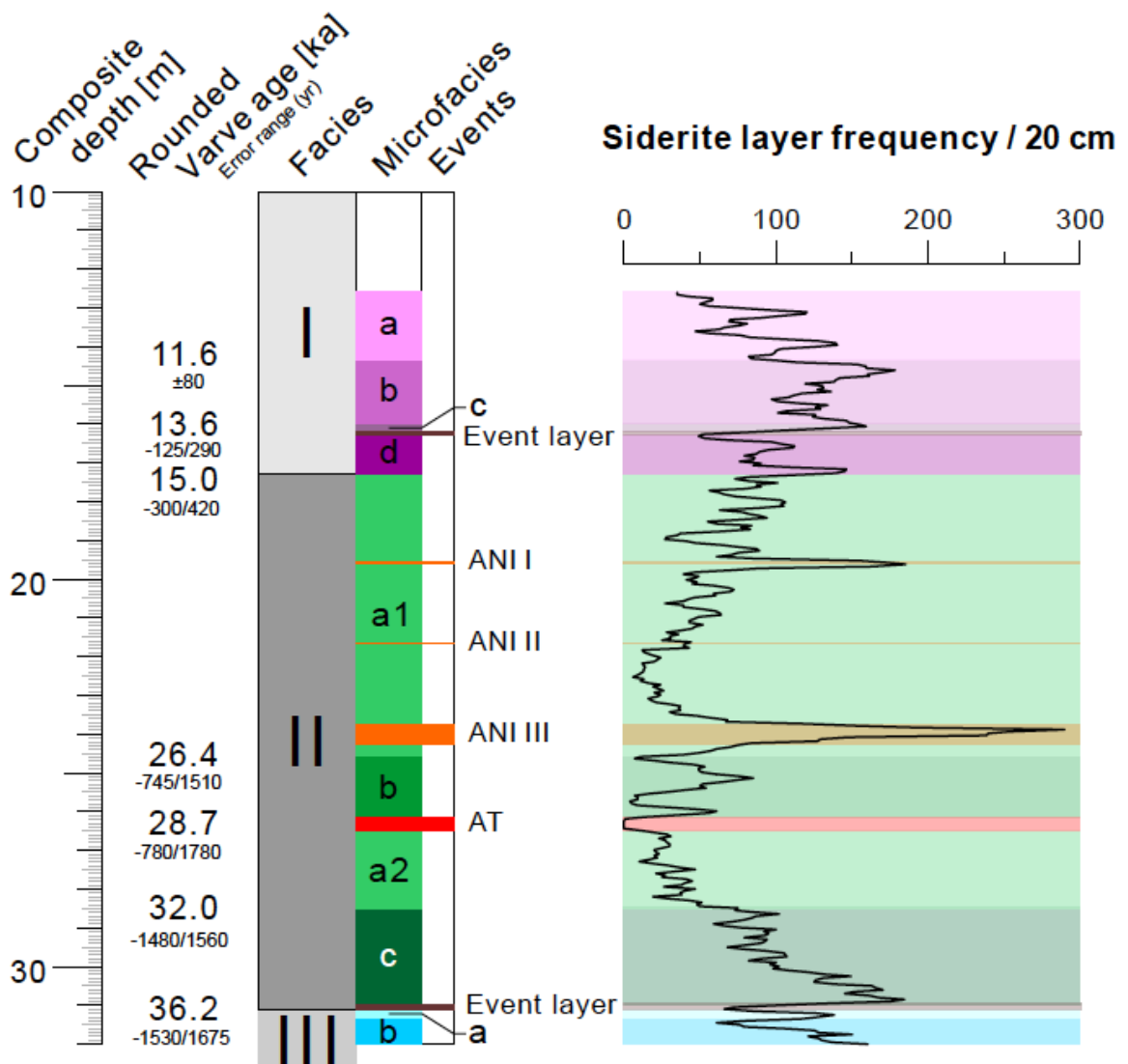
1280 √ Fig. 4 a and b. Atmospheric ^{14}C ages and plateaus (horizontal boxes) deduced from
 1281 ^{10}Be production rates vs. GICC05 age scale (Adolphi et al., 2018) compared to the
 1282 Suigetsu record of atmospheric ^{14}C plateaus vs. Hulu U/Th-based model ages (Southon
 1283 et al., 2012; Cheng et al., 2018) for the intervals a) 10-20 and b) 19-29 cal ka BP.





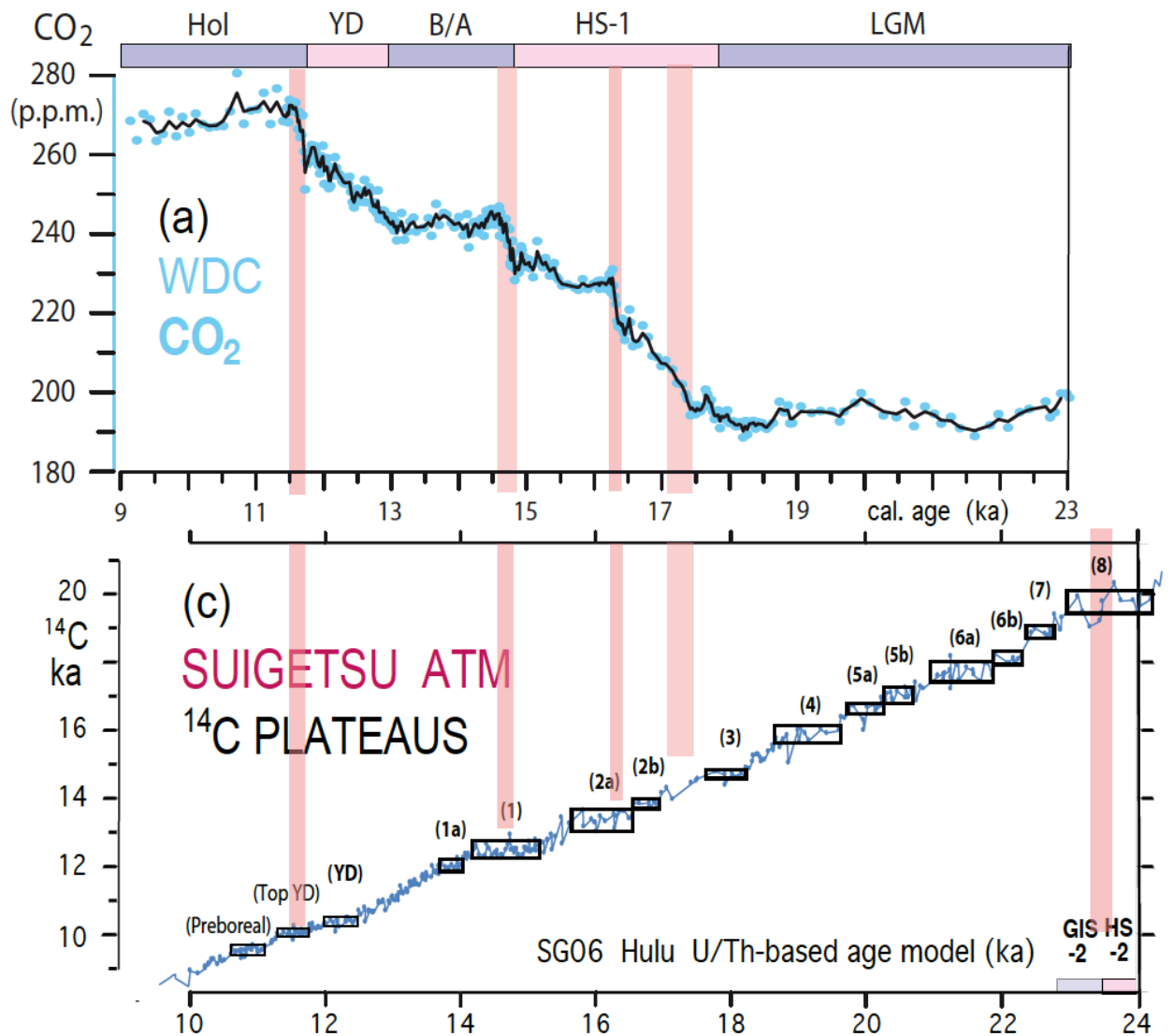
1285
 1286
 1287
 1288
 1289
 1290
 1291
 1292
 1293
 1294
 1295
 1296
 1297
 1298

1299 √ Fig. 5. Sediment facies and microfacies zones in Lake Suigetsu Core SG06, ~13–32
 1300 m depth (simplified and suppl. from Schlolaut et al., 2018). Microscopy-based frequency
 1301 of siderite layers with quality level 1–3 (= running average of layer counts per 20 cm
 1302 thick sediment section) serves as measure of seasonal lamination quality and shows
 1303 gradual transitions between varved and poorly varved sediment sections. Rounded
 1304 varve ages are microscopy based and constrain age of major facies and microfacies
 1305 boundaries. ANI I to ANI III mark core sections with ultrafine lamination due to
 1306 sedimentation rate minima, AT marks tephra layer named AT, ‘Event layers’ label major
 1307 thin mud slides probably earth quake-induced.s



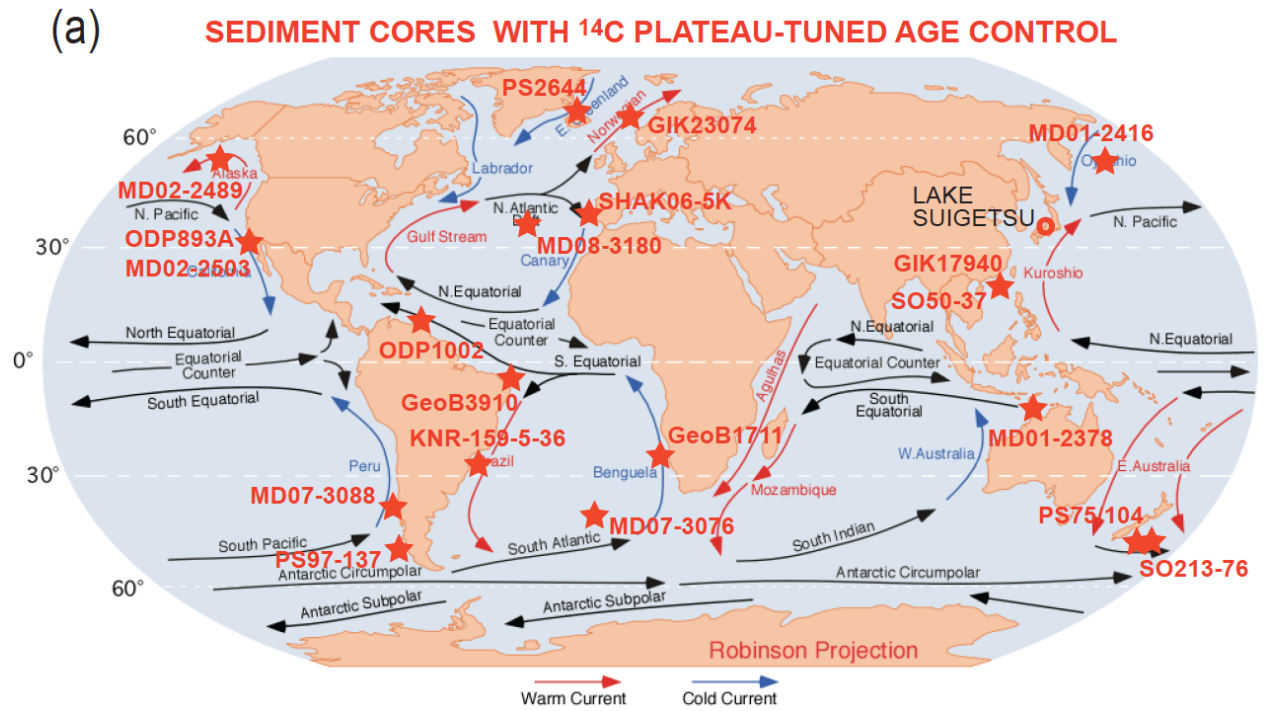
1308

1309 √ Fig. 6 (a). Four sudden steps (pink bars) in the deglacial atmospheric CO₂ rise at
 1310 West Antarctic Ice Sheet Divide ice core (WDC) reflect events of fast ocean degassing,
 1311 that may have contributed to the origin of deglacial ¹⁴C plateaus. Age control based on
 1312 ice cores (Marcott et al., 2014). (b) The steps are compared to suite of atmospheric ¹⁴C
 1313 plateaus dated by Hulu U/Th-based model ages (Bronk Ramsey et al., 2012). Hol =
 1314 Holocene; YD = Younger Dryas; B/A = Bølling-Allerød; HS = Heinrich stadials 1 and 2;
 1315 LGM = Last Glacial Maximum, GIS-2 = Greenland interstadial 2.
 1316

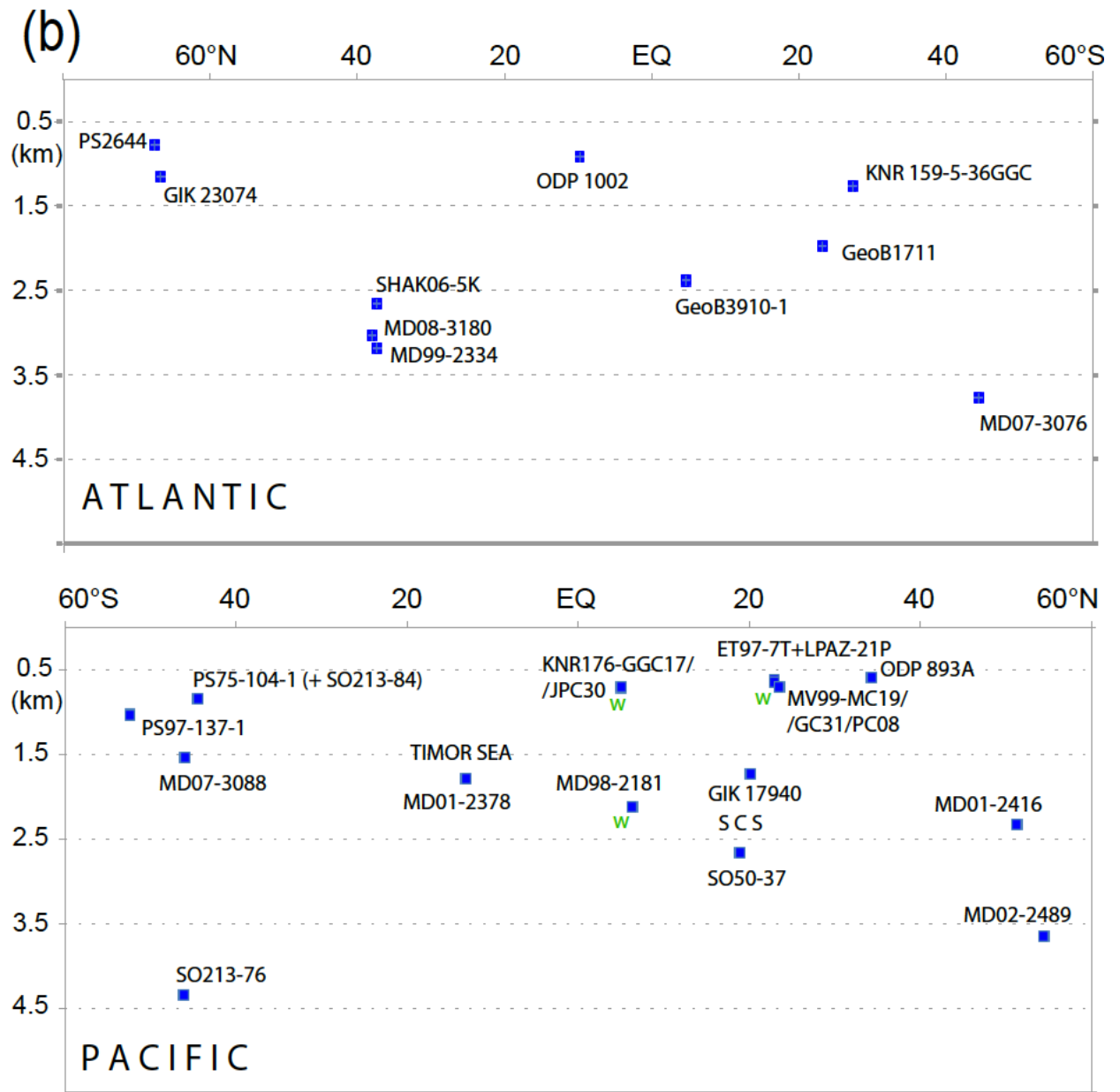


1317
 1318

1319 √ Fig. 7. Location (a) and water depth (km) (b) of sediment cores with age control based
 1320 on ^{14}C plateau tuning. ^{14}C reservoir ages of cores labeled with 'w' are derived from
 1321 samples with paired wood chunks and planktic foraminifers.



1322



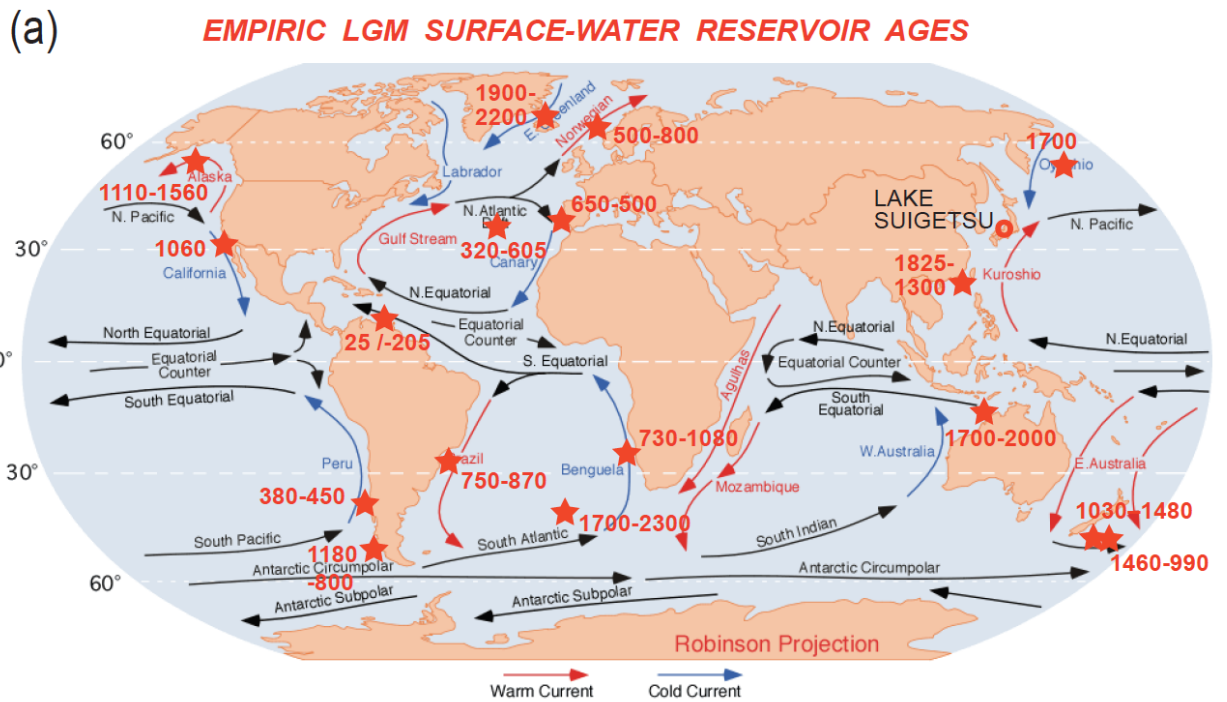
1323

1324

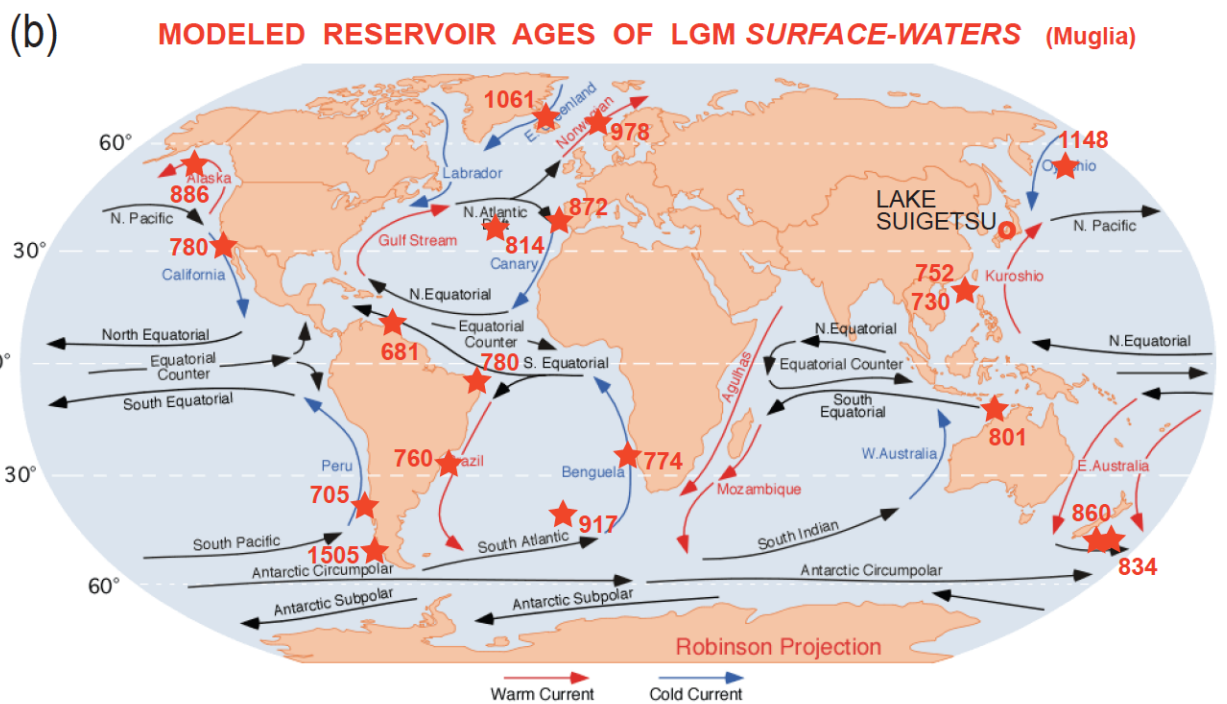
1325 √ Fig. 8. Global distribution of ^{14}C reservoir ages of Late LGM surface waters estimated
 1326 (a) by means of ^{14}C plateau tuning of planktic ^{14}C records. (b) Model-based estimates
 1327 (GCM of Muglia et al., 2018, assuming an AMOC strength of 13 Sv) for sites with
 1328 planktic foraminifera-based age values. X-Y graph (c) and map (d) show (rounded)
 1329 differences between observed and modeled values and their intra-LGM trends. Minor
 1330 differences are displayed in magenta, larger differences of >400 yr in red. Planktic
 1331 habitat depths and model estimates are largely confined to 0–100 m water depth.

1332 Arrows of surface currents delineate different sea regions important to assess potential
 1333 limits of spatial extrapolation of reservoir ages. Distribution of core numbers and
 1334 references for ¹⁴C records are given in Table 3a-c and Fig. 7a.

Fig. 8a

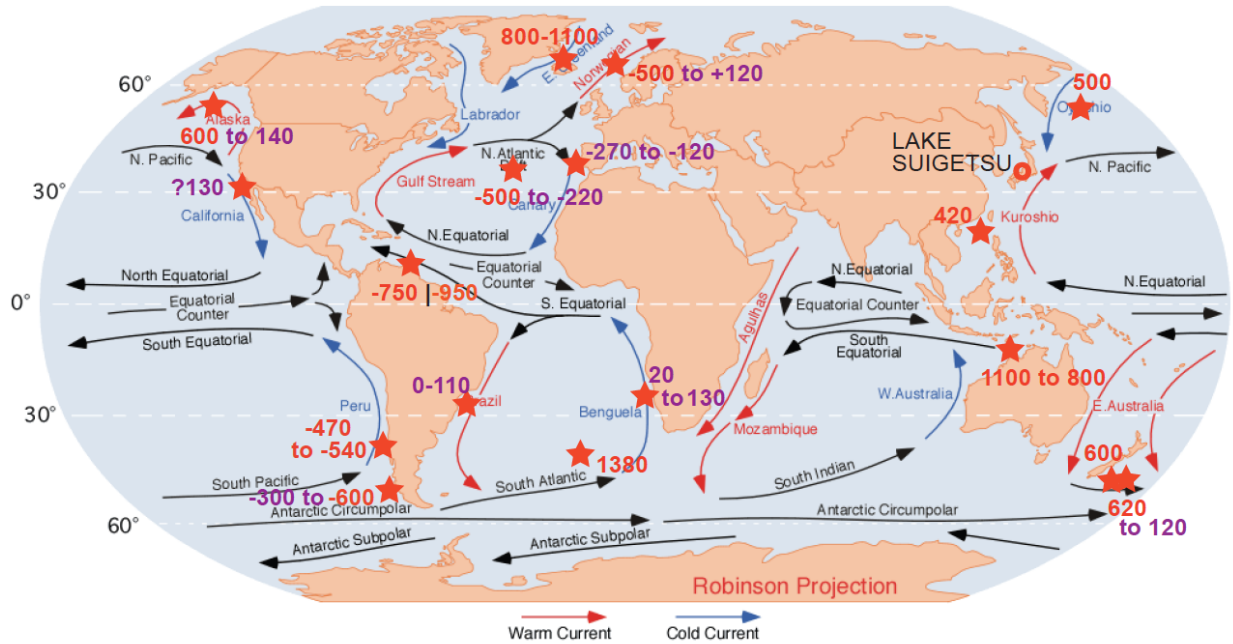


1335



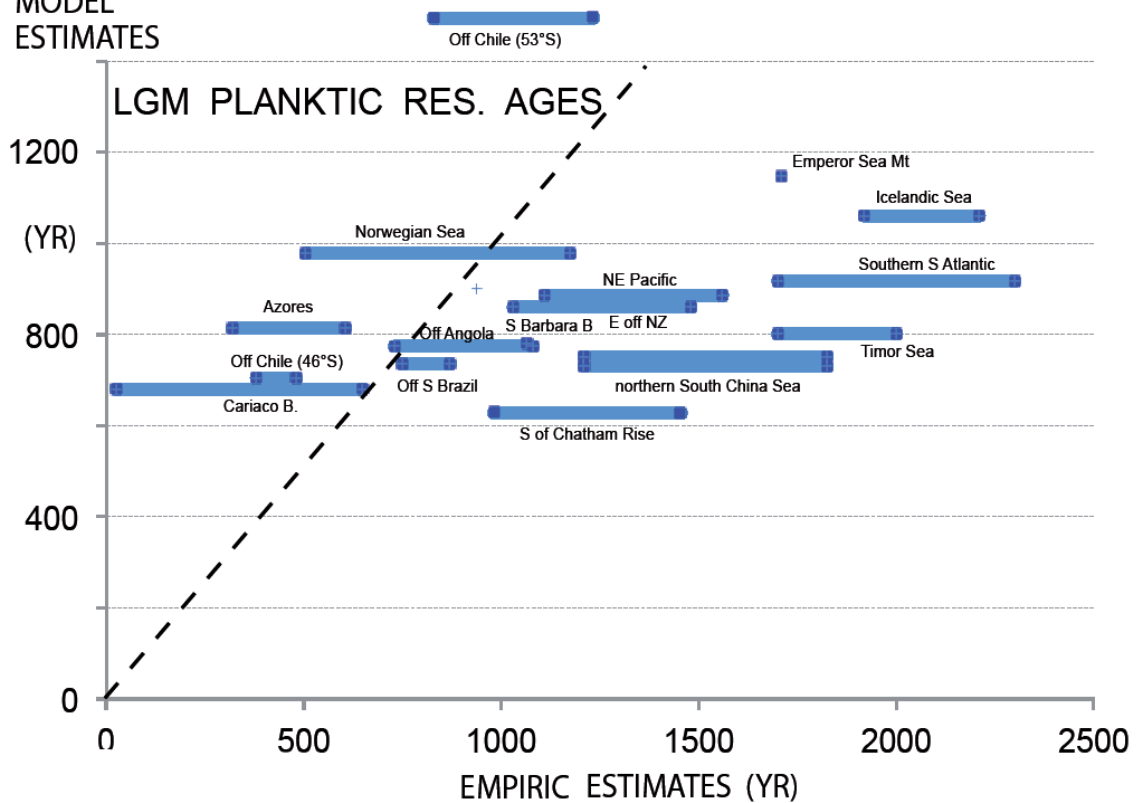
1336

(c) **EMPIRIC minus Muglia MODEL RESERVOIR AGES (yr) of LGM S.W.**



1337

(d) **MODEL ESTIMATES**

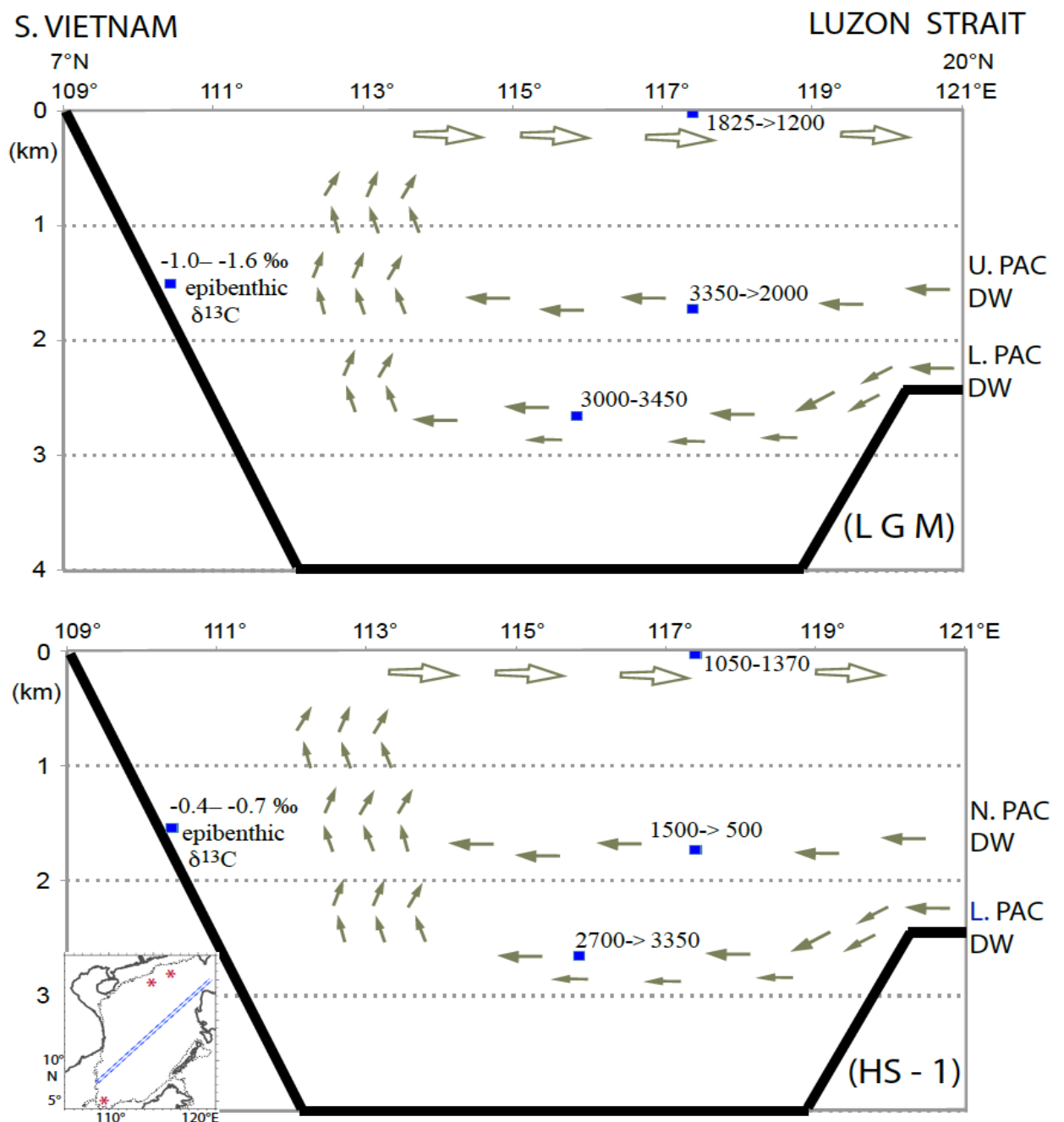


1338

1339

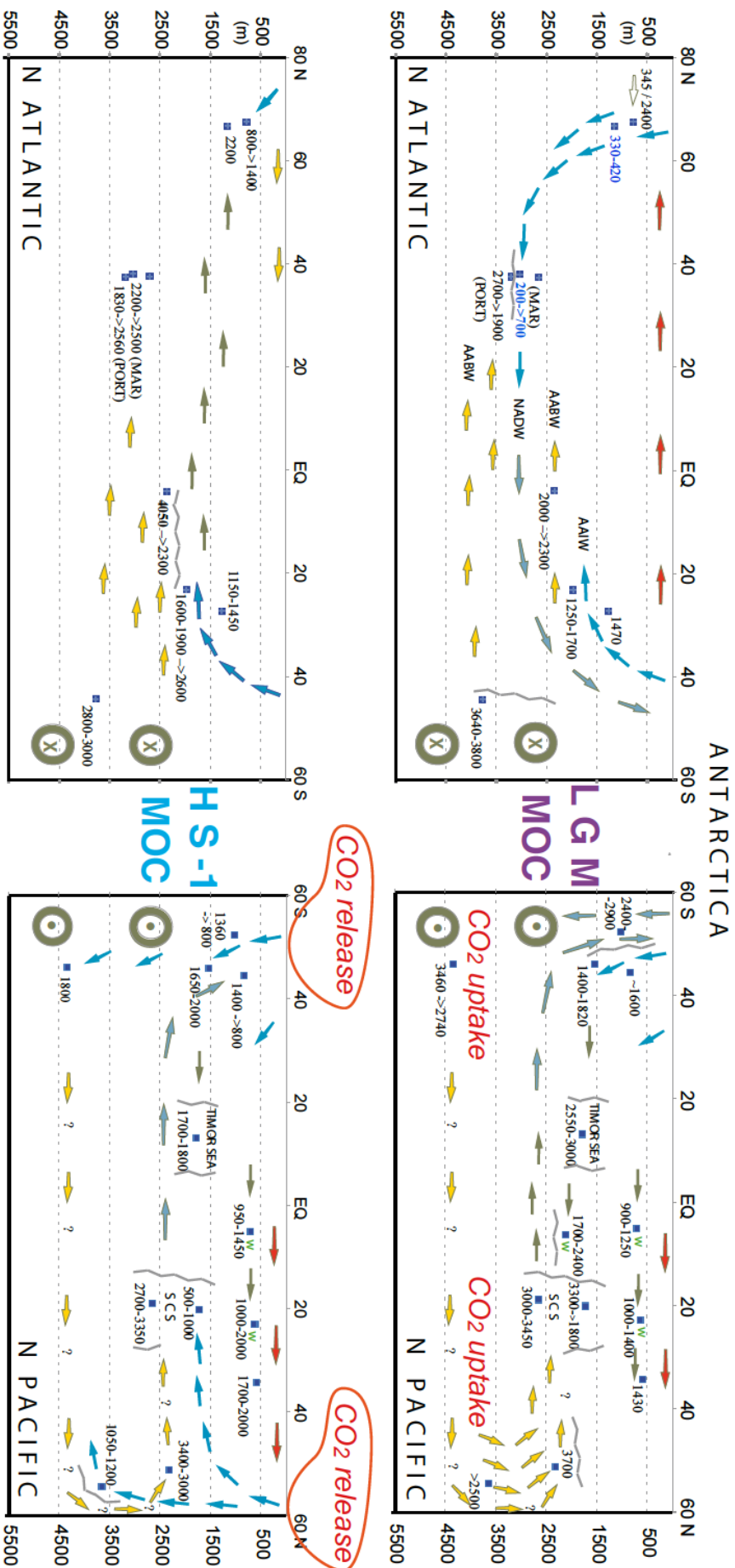
1340 √ Fig. 9. SW–NE transect of ^{14}C reservoir age and changes in ventilation age across
 1341 sites GIK17940 and SO50-37 in the South China Sea during late LGM (^{14}C Plateaus 5

1342 and 4; upper panel) and HS-1 (lower panel). Insert map shows location of transect and
 1343 core locations. Core locations are given in Fig. 7. An extreme epibenthic $\delta^{13}\text{C}$ minimum
 1344 in far southwest (Core GIK17964; Sarnthein et al., 1999) reflects an LGM incursion of
 1345 Lower/Upper Pacific Deep Waters (L./ U. PAC DW) with extremely high ^{14}C ventilation
 1346 age and DIC enrichment in contrast to a low ventilation age of North Pacific Deep Water
 1347 (N. PAC DW). Arrows show direction of potential deep and intermediate-water currents.



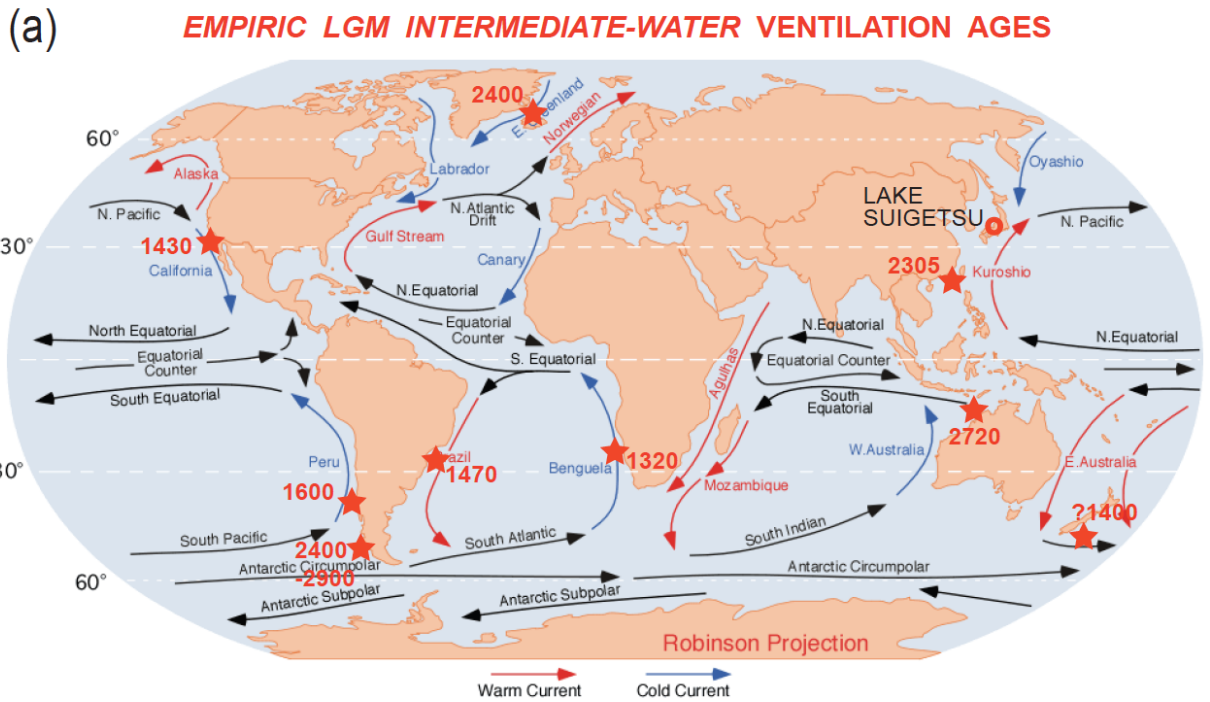
1348

1349 √ Fig. 10. 2D transects of the geometries of global ocean MOC. Arrows (blue = high,
1350 yellow = poor ventilation) suggest average deep and intermediate-water currents that
1351 follow the gradient from low to high benthic ventilation ages based on paired planktic
1352 ¹⁴C reservoir ages derived by means of ¹⁴C plateau tuning technique (Sarnthein et al.,
1353 2013, Balmer et al., 2018, Küssner et al., under review). At some Pacific sites reservoir
1354 ages are based on paired ¹⁴C ages of planktic foraminifera and wood chunks (marked
1355 by green 'w'; Sarnthein et al., 2015; Zhao and Keigwin, 2018, Rafter et al., 2018). Red
1356 arrows suggest poleward warm surface water currents. Zigzag lines indicate major
1357 frontal systems separating counter rotating ocean currents (e.g., W of Portugal and N of
1358 MD07-307; after Skinner et al., 2014). (a) Late LGM circulation geometry (21–18.7 cal.
1359 ka), largely similar to today. Note the major east-west gradient of ventilation ages in the
1360 central North Atlantic, between Portugal (PORT) and Mid-Atlantic Ridge W of Azores
1361 (MAR). (b) HS-1 benthic ventilation ages reveal a short-lasting MOC reversal leading to
1362 Atlantic-style overturning in the subpolar North Pacific and coeval Pacific-style stratific-
1363 ation in the northern North Atlantic, with seesaw-style reversals of global MOC at the
1364 onset and end of early HS-1 (first proposed by Broecker et al., 1985, however, for LGM
1365 times). Increased ventilation ages reflect enhanced uptake of dissolved carbon in the
1366 LGM deep ocean (Sarnthein et al., 2013), major drops suggest major degassing of CO₂
1367 from both the deep Southern Ocean and North Pacific during early HS-1. – SCS =
1368 South China Sea. AABW = Antarctic Bottom Water; AAIW = Antarctic Intermediate
1369 Water. NADW = North Atlantic Deep Water. Small arrows within age numbers reflect
1370 temporal trends. Many arrows are speculative using circumstantial evidence of benthic
1371 δ¹³C records and local Coriolis forcing at high-latitude sites per analogy to modern
1372 scenarios. Location of sediment cores are given in Fig. 7, short-term variations in
1373 planktic and benthic ¹⁴C reservoir/ventilation age in Suppl. Fig. S2 and Table 3.

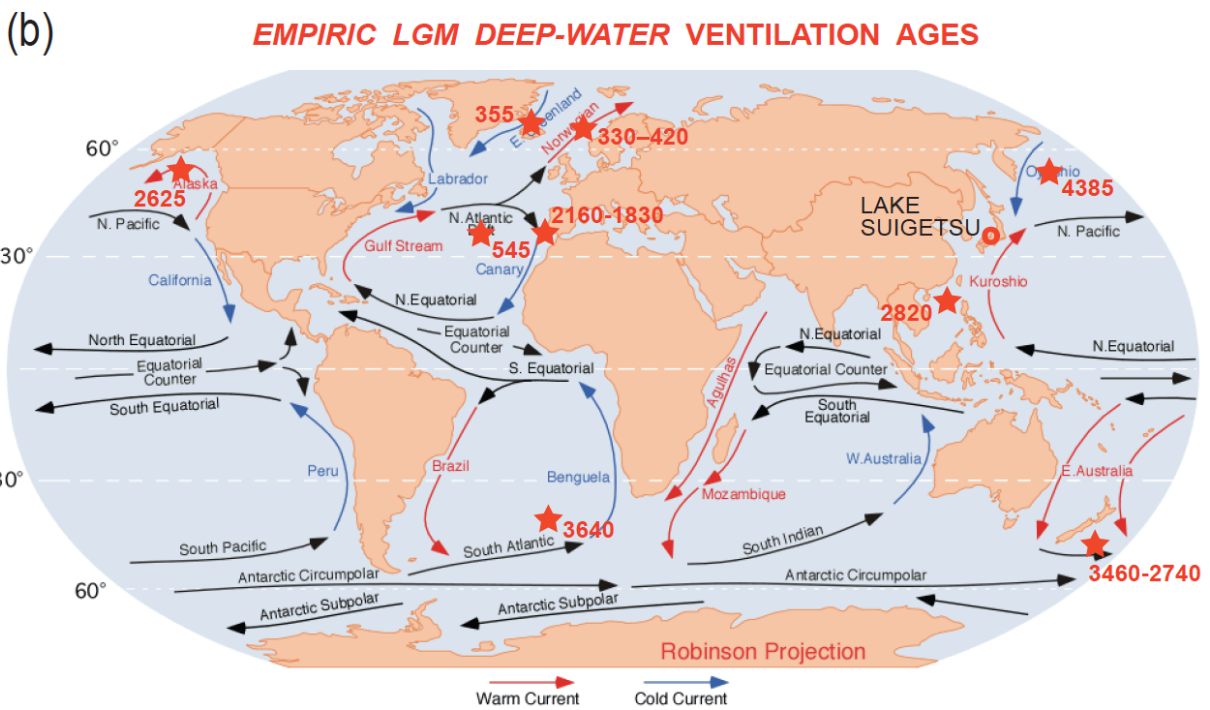


1375

1376 √ Fig. 11. Global distribution of ¹⁴C reservoir ages obtained (a) for late LGM
1377 intermediate waters (100–1800 m w.d.) and (b) for LGM deep waters (>1800 m w.d.,
1378 including Site GIK 23074 at 1157 m in the Norwegian Sea).



1379



1380